(2)

CHEMICAL RESEARCH, DEVELOPMENT & ENGINEERING CENTER

CRDEC-CR-113

DEVICE FOR SORTING MICRON SIZE DIELECTRIC AND CONDUCTING POWDERS

Madhau B. Ranade
Ruijng Han
James W. Gentry

PARTICLE TECHNOLOGY, INC.
College Park, MD 20742

August 1991

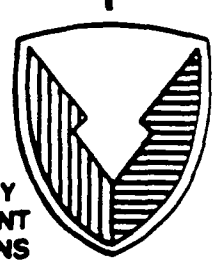

U.S. ARMY
ARMAMENT
MUNITIONS
CHEMICAL COMMAND

Aberdeen Proving Ground, Maryland 21010-5423

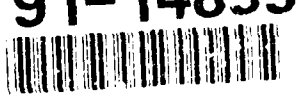

Disclaimer

The findings in this report are not to be construed as an official Department of the Army position unless so designated by other authorizing documents.

REPORT DOCUMENTATION PAGE

Form Approved
OMB No. 0704-0188

1. AGENCY USE ONLY *(Leave blank)*	2. REPORT DATE	3. REPORT TYPE AND DATES COVERED
	1991 August	Final, 90 Aug - 91 Feb

4. TITLE AND SUBTITLE
Device for Sorting Micron Size Dielectric and Conducting Powders

5. FUNDING NUMBERS
C-DAAA15-90-C-1065
CDRL A0001

6. AUTHOR(S)
Ranade, Madhau B.; Han, Ruijng; and Gentry, James W.

7. PERFORMING ORGANIZATION NAME(S) AND ADDRESS(ES)
Particle Technology, Inc.
Building 335, Paint Brush Dr.
College Park, MD 20742

8. PERFORMING ORGANIZATION REPORT NUMBER
CRDEC-CR-113

9. SPONSORING/MONITORING AGENCY NAME(S) AND ADDRESS(ES)
CDR, CRDEC, ATTN: SMCCR-RSB-B, APG, MD 21010-5423

10. SPONSORING/MONITORING AGENCY REPORT NUMBER

11. SUPPLEMENTARY NOTES
COR: C.L. Cash, SMCCR-RSP-B, (301) 671-4294

12a. DISTRIBUTION/AVAILABILITY STATEMENT
Approved for public release; distribution is unlimited.

12b. DISTRIBUTION CODE

13. ABSTRACT *(Maximum 200 words)*

A laboratory classifier was designed and fabricated to classify several test powders in the micron and submicron size range. These powders represent both conducting and dielectric media. The classifier is based on an inertial and electrical separation and sorting of particles according to the particle size. Test particles of known size characteristics were used to determine the performance of the devices.

14. SUBJECT TERMS			15. NUMBER OF PAGES
Particles	Shape	Size	72
Classification	Inertia		16. PRICE CODE
Electrostatics	Charging		

17. SECURITY CLASSIFICATION OF REPORT	18. SECURITY CLASSIFICATION OF THIS PAGE	19. SECURITY CLASSIFICATION OF ABSTRACT	20. LIMITATION OF ABSTRACT
UNCLASSIFIED	UNCLASSIFIED	UNCLASSIFIED	UL

Blank

PREFACE

The work described in this report was authorized under Project No. DAAA15-90-C-1065. This work was started in August 1990 and completed in February 1991.

The use of trade names or manufacturers' names in this report does not constitute an official endorsement of any commercial products. This report may not be cited for purposes of advertisement.

This report has been approved for release to the public.

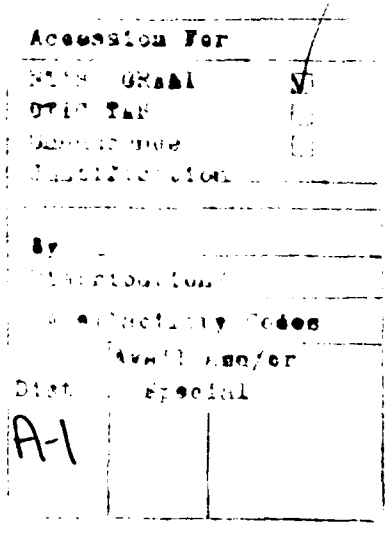

Blank

CONTENTS

LIST OF FIGURES

LIST OF TABLES

Blank

DEVICE FOR SORTING MICRON SIZE DIELECTRIC
AND CONDUCTING POWDERS

1. INTRODUCTION

Particles in the micron and submicron size range are used for various applications such as obscuration smokes, coatings, ceramic, and composite materials. It is often desirable to use particles of specific size and shape to maximize the performance potential of smokes or other materials. Preparation of custom particles for these applications is usually expensive because of the "one-of-a-kind" apparatus and processes required and the high level of technical expertise necessary.

A device to sort (or to classify) particles in these micrometer and smaller size ranges would represent a reasonable solution since inexpensive, commonly available materials such as pigments and other powders containing a broader size distribution may be used as the starter material. However, most commercial devices, such as centrifugal classifiers, separate particles aerodynamically and are inherently limited to sort in larger size ranges.

In addition to the lower size range, the proposed device would also be effective for separation of particles according to shapes such as flakes and needles since the extent of electrical charge strongly depends on the total surface area. Both dielectric and conducting particles can be charged and sorted by this technique.

1.1 Phase I Technical Objective

The general objective of the Phase I effort is to demonstrate feasibility of the combination aerodynamic/electrostatic classifier. The specific objectives of the effort are:

1. To develop a theoretical basis for charging and classification of particles of different shapes in the micrometer and submicrometer size ranges.

2. To fabricate a simple apparatus to experimentally verify classifier performance, and

3. To process several samples supplied by the Army along with performance data.

1.2 Particle Size and Shape Classifiers

Particle classification by size in the micrometer size range is carried out by aerodynamic means and, because of low inertia, particle smaller than $1 - 3\mu m$ cannot be easily sorted. Allen (1981) presents a comprehensive summary. A commercial classifier made by the Nisshin company approaches this limit. Yamada et al (1987) extended its performance down to $0.5\mu m$ by operating the whole system in an evacuated chamber.

In order to sort or classify particles by size and or shape in the submicrometer range the combination of electrical and mechanical mechanisms might be useful. Leschonski (1987) describes the feasibility of particle separation in a centrifuge in the presence of an electrical field shown schematically in figure 1.1. Classification takes place in the annular gap between two cylinders rotating at the same angular speed. The aerosol particles are introduced at the top at an intermediate radius

$$R = \frac{(R_1 + R_2)}{2}$$

The axial distance L is

$$L = \frac{2Rnv}{v}$$

where v is the velocity in the axial direction, n is the number of revolutions by the rotors.

The electrical field in the annulus is given by

$$E = \frac{U}{Rln(R_1/R_2)}$$

where U is the high voltage potential between the cylinders. The migration of the particle is calculated using the relation

$$w = \frac{EqCu}{3d}$$

The displacement in the centrifugal field is calculated by a force balance between the centrifugal force and fluid drag. The overall distance travelled by a particle is the algebraic sum of the displacement by the electrical and centrifugal mechanisms. Leschonski (1987) solved several cases using different voltages, speeds of rotation and particle sizes. An example is shown in figure 1.2. It should be noted that $l = 0$ represents the particle which did not move from the center of the gap and is the "cut" diameter. In general the more the number of cycles the sharper is the size classification.

Particle sorting by shape has not been studied except by people interested in hazardous fibers such as asbestos. Use of an electrical field for aligning fibers on substrates for microscopy has been reported but quantitative information is not available. Use of other techniques in liquid media is possible but has not been seriously studied to develop a sorting device.

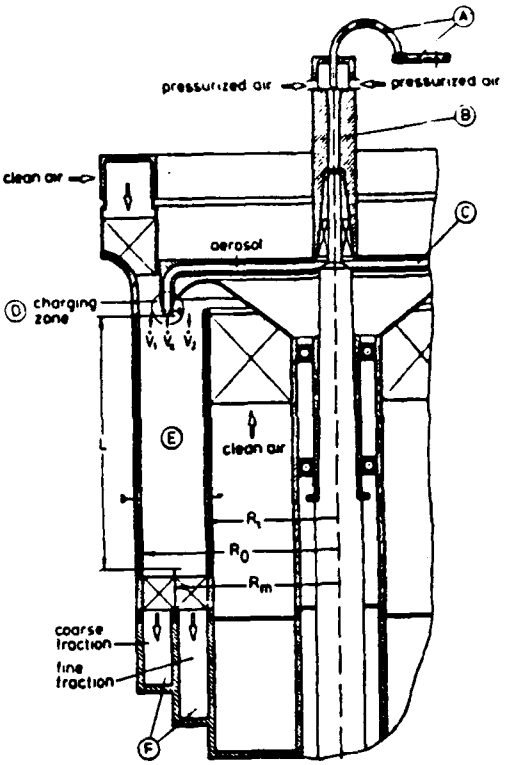

Figure 1.1 Schematic Drawing of Electrostatic Classifier (Leschonski, 1987)

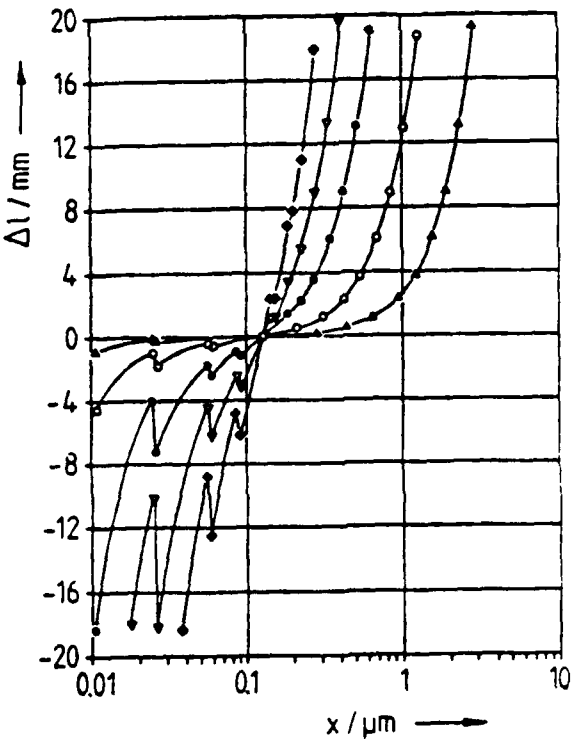

Figure 1.2 Displacement for Different Number of Cycles(n) (Leschonski, 1987)

1.3 Phase I Concept of the Sorting Device

A laboratory classifier was designed and fabricated to classify several test powders in the micron and submicron size range and representing conducting and dielectric media. The classifier was based on electrostatic separation and sorting of particles according to particle size and aspect ratio. The performance was evaluated using test particles of known size characteristics and by measuring size characteristics of the sorted particles. Design information for the Phase II prototype was developed using a parametric test sequence.

After consultation with the Army CRDEC staff, four powders were included initially in the project for design consideration. These include submicrometer TiO_2, Carbon fibers, Carbon flakes, and Iron fibers. Since TiO_2 is primarily isometric in shape only inertial separation is important. The first three powders were therefore included in the electrostatics investigation.

In a project meeting with Army COR it was decided that aerodynamic separation might be useful before the electrostatic sorting. Separate section for each separation scheme shown in figure 1.3 is permissible and might even be preferable.

SORTING SEQUENCE

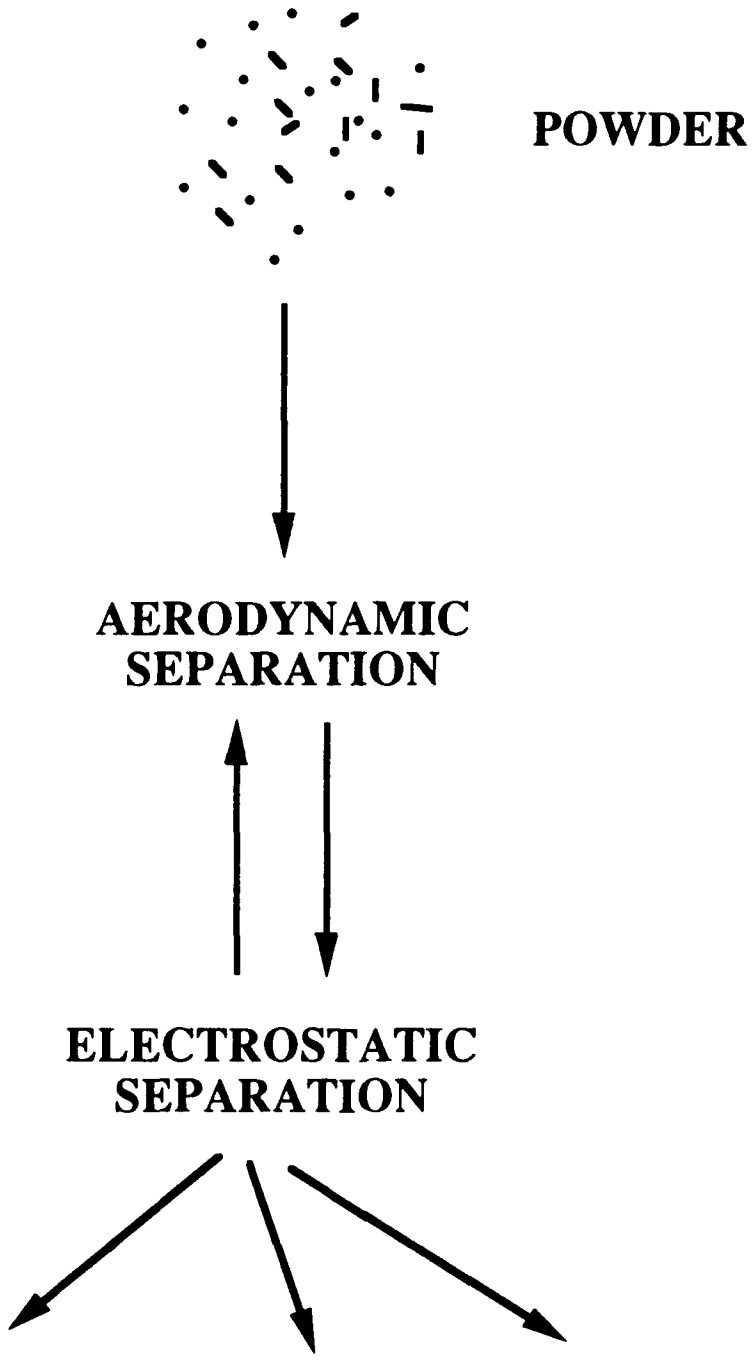

Figure 1.3 Sequence for Sorting Particles by Size and Shape

2. CHARGING OF NON-SPHERICAL PARTICLES

The charging of the particles was assumed to be in diffusional mechanism regime. The particles acquire charge by the collision of ions with the particle. The movement of the ions is due to thermal or Brownian motion. However, as the particle acquires charge, the Coulombic potential between the particle and the ion, inhibits the acquisiton of additional charges. Based on this model, several investigations showed that the charge distribution on large particles could be described by a Boltzmann distribution. Since, in general, the ion mobilities of positive and negative ions differ, it was necessary to correct the distribution for unequal mobilities. Such corrections were made by Gunn(1955), and as a consequence the agreement between theoretical and experimental charge distributions were close.

However, as the particles became smaller, the experimental charge distribution indicated that the particles were much more heavily charged than calculated from theory. This discrepency was explained by indicating that the ion flux to the particle could no longer be explained by treating the gas around the particle as a continuum. Several computational approaches were suggested. In one class of approaches, the particle is surrounded by a hypothetical bounding surface. Outside the surface, the system is treated as a continuum. Within the boundary the particle-ion interaction is treated with a trajectory calculation of the ion. Kinetic energy and angular momentum are conserved. In the second approach the system is handled as a rarefied gas. The Boltzmann equation is solved. The flux of ions to the particle are then obtained by integration along

lines of constant characteristics.

If the particle were a perfect conductor and if the potential on the particle surface is to remain constant as the charge approaches the particle , it is necessary to introduce a hypothetical "image" charge. The potential between the charge and the "image" term is inversely proportional to the distance between the charge and the particle surface. This implies that the potential and consequently the force between the charge and the particle would approach infinity(figure 2.1). Consequently, it was necessary to introduce a convention to avoid the singularity at the particle surface. Three classes of approaches were taken,

(1) The particle was enclosed in a bounding surface, outside the surface the particle -ion dynamics were treated as a continuum. (Fuchs(1968), Hoppel(1975))

(2) The system was treated as a rarefied gas with the flux determined by solutions of the Boltzmann equation. An additional physical constraint (i.e. minimization of flux , preservation of kinetic energy , etc.) was imposed. (Gentry(1972) , Marlowe(1975)) or

(3) The image term was neglected and a modified boundary condition was imposed at the surface. Essentially the boundary condition was constrained to be consistent with the solution of the Boltzmann equation. (Laframboise and Chang(1973a, b))

Calculations have been carried out for spherical particles using all three approaches. The equilibrium charge distribution for bipolar charging was es-

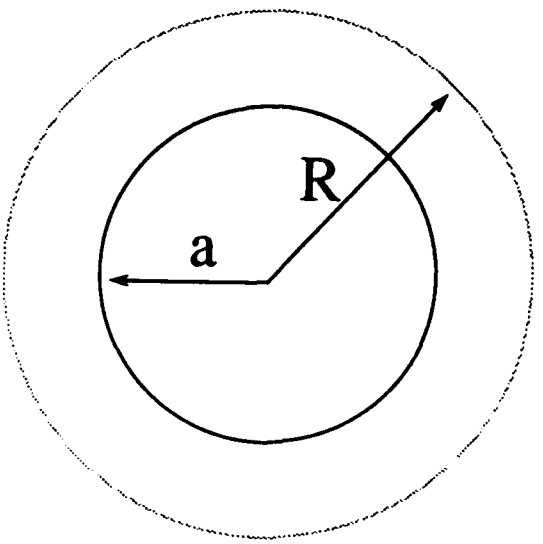

$$N \sim \exp\left(-\frac{e^2}{akT}\left[\pm\frac{1}{\bar{R}} - \frac{1}{2\bar{R}^2(\bar{R}^2-1)}\right]\right)$$

N - Ion Flux

$\bar{R} = R / a$

Figure 2.1 Schematic and Ion Flux of Spherical Particles

sentially the same for each of the approaches. They all predicted rough agreement with the Boltzmann equilibrium for larger particles and they predicted a significantly higher charge for particles less than $50nm$. The predicted charge distribution agreed with experimental determinations within uncertainty in the magnitude of physical constants (i.e. ratio of ion mobilities, absolute value of ion mobilitly, etc.). Similar calculations were carried out for the rate of unipolar charging. These indicate a substantial difference between the first two approaches and the third approach where the image correction is neglected. The limited experimental measurements strongly suggest the necessity of including the image correction.

There are two logical extensions of the calculations with spherical particles : the dynamic regime can be extended into the transition and slip flow regimes and the geometry of the particle can include non-spherical shapes. Neither of the extensions are trivial. An approach based on a linearization of the Boltzmann equation has been carried out for spherical particles. There was little change in the charge equilibrium , and relatively small change in the rate of charging. The approaches for different geometries represent a significant feature of this report and are discussed below.

2.1 Model Fiber

The principal criteria in developing a model for the diffusional charging of fibers are the following :

1. The geometry of the model must closely resemble the fiber and cover a range of aspect ratioes from 3 upwards ,

2. The Coulombic potential between the charge on the particle and an external charge must be expressed in closed form,

3. The image correction must be represented in closed form , and

4. The aerodynamic drag must be expressed in closed form.

We selected a "capped cylinder" model for modeling fibers. This model consist of three sections - a cylindrical mid-section of length $(B-1)D$ and diameter D capped by two hemispheres of diameter D. This model collapses to a sphere as $B-1$ approaches zero, and approaches a cylinder for large aspect ratios. The "image correction" can be expressed in closed form for only a limited number of special cases; however two of the cases are cylinders and spheres. Moreover the Coulombic potential between an external charge and a sphere can be expressed as the interaction between the external charge and a hypothetical charge located at the center of the sphere. The Coulombic charge between an external charge and a cylinder can be expressed as the interaction between the charge and a line charge along the central axis of the cylinder. Thus the "capped cylinder" model incorporates the best features of models based on a prolate spheroid and a cylinder .

A diagram of the model and the expressions for the potential beween a charge and the fiber are shown in figure 2.2. In this model the space around the fiber is divided into three zones. The middle zone is bounded by a concentric cylinder of length $(B-1)D$ and diameter KD. The two end zones are hemispheres with a diameter KD. Thus the bounding zone is a stumpier version of the original fiber. The expression for the Coulombic potential can then be

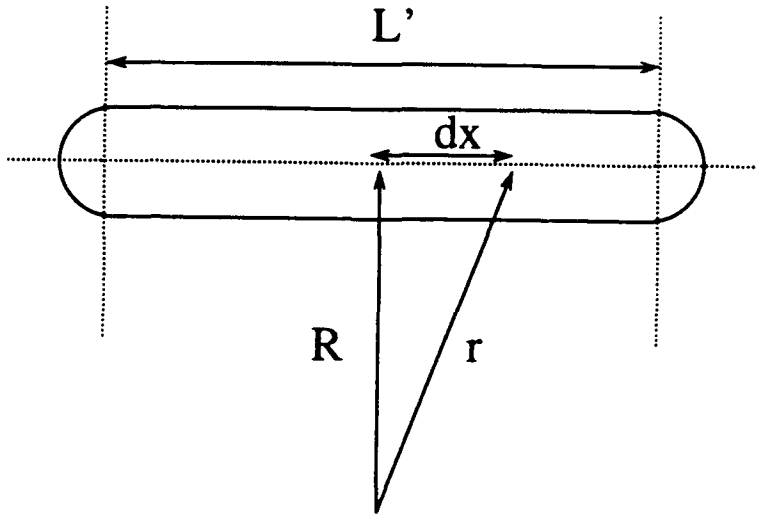

$$\phi_c = \frac{2\,qJ\psi_0}{b}\,\mathrm{Ln}\{\,(b+\sqrt{b^2+R^2})\,/\,R\,\}\;-\;\frac{\psi_0}{2\,R^2\,(R^2-1)}$$

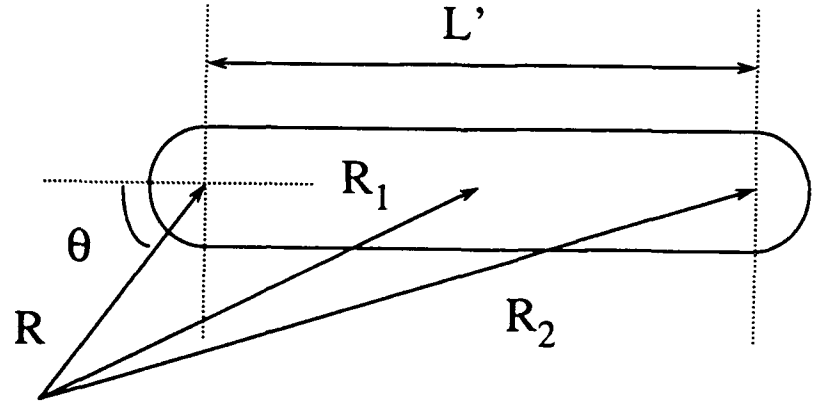

$$\phi_s = \frac{qJ\psi_0}{b+1}\left(\,1 + 1/4b + (b+1)/R - \sqrt{1+b^2/R^2} - 1/4b\sqrt{1+4b^2/R^2}\,\right) - \frac{\psi_0}{2\,R^2\,(R^2-1)}$$

$$b = \beta - 1$$

Figure 2.2 Schematic and Ion Flux of Cylindrical Fiber

expressed for any location of the charge. If the charge lies within one of zones bounded by hemispherical caps - the interaction is represented as the sum of three terms corresponding to point charges at the focii of the two hemispherical sections and at the center of the cylindrical section. The charge is assumed to be uniformly distributed over the surface area of the particle. If the charge lies in the zone bounded by the cylinder, the charge on the particle is treated as a line source having a uniform charge.

To summarize, the charging model (shown in figure 2.2) consists of a cylinder capped by two hemispherical caps. The bounding surface has the same structure , although the length of the cylindrical section remains the same. The charge on the particle is assumed to be uniformly distributed over the particle surface. It is approximated by either three point sources (in the hemispherical zones) or by a line source (in the cylindrical zone). The image correction which is a known, analytical function for spheres and cylinders is incorporated into the potential.

The diameter of the bounding surface KR is determined by the minimum flux method. The flux is integrated along lines of constant characteristics from $R \rightarrow \infty$ to $R = KR$. The total flux is then determined as the product of the radially dependent flux and the surface area. As $K \rightarrow 1$ (i.e. the charge approaches the particle surface) the potential and consequently the force increases without bound. This infinite attraction is manifest in unbounded values for the kinetic energy and the flux normal to the surface. It is to prevent these physically unrealistic conditions that a bounding surface must be introduced. In the

simulations below the criterion was that the total flux was a minimum. (This means that the bounding surface excludes the generation of charge within the the bounding surface).

2.2 Model Platelet

The schematic of the platelet is shown in figure 2.3. The bounding surface in this case is represented by a cylinder with the disc cross - section at a distance Z from the center axis of the platelet. This model is not completely satisfactory. There are two difficulties - the potential treats the particle as an oblate spheroid for the Coulombic potential and as a flat plate for the image correction and the diameter of the bounding cylinder. For unipolar charging where in general the particle and ions have the same charge , there will be a repulsion so that the effective disc cross- section is less than that of the particle. The problem arises when the particle and ion have different polarities and there is a net attraction. In this case the disc diameter will vary with the distance from the center plane of the particle.

In the simulations reported below we consider the case of unipolar charging implying a net repulsion between the ions and the particle . In this case treating the bounding volume as the surface is adequate.

2.3 Numerical Simulation

The numerical simulation was designed to approximate the behavior of the unipolar charger. The ion flux to the aerosol was determined from the " minimum flux " criterion . In this model the rate of charging is proportional to the ion density and the ion velocity. In the simulations the ion velocity

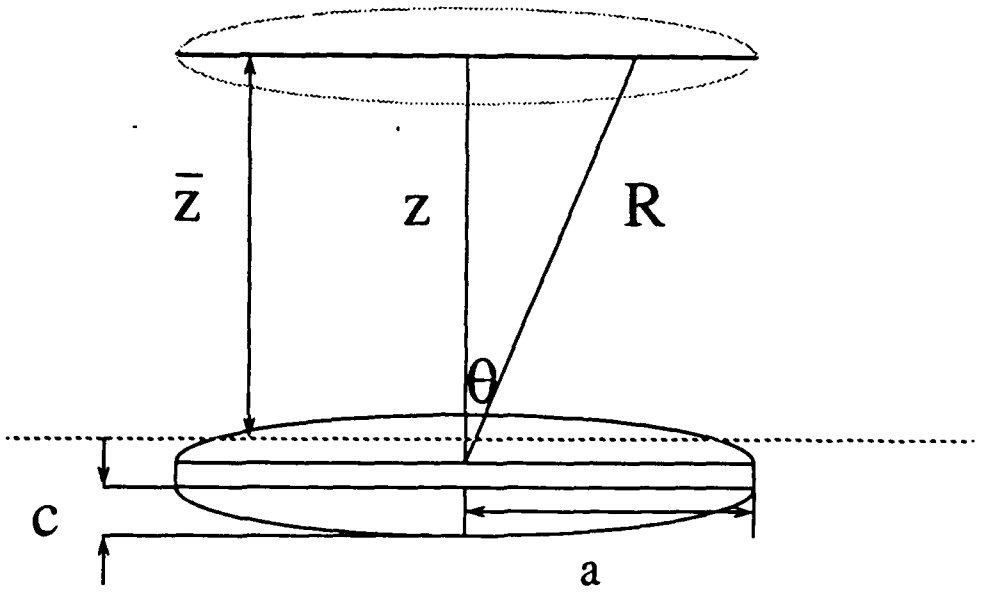

$$z^* = z - \frac{2}{3}\,c$$

$$\phi^* = \left(\frac{qJ\psi_0}{\sqrt{1-\beta^2}} \tan^{-1} \sqrt{\frac{1-\beta^2}{R(\bar{z},\theta)}} \right) - \frac{\psi_0}{2\,\bar{z}^*}$$

$$\text{Flux} \sim \frac{\displaystyle\iint_0^{\tan^{-1} a/z} \exp(-\phi^*)\cos\theta\sin\theta\, d\theta\, d\varphi}{\displaystyle\iint_0^{\tan^{-1} a/z} \sin\theta\, d\theta\, d\varphi}$$

$$\beta = c/a\,, \quad \bar{z} = z/a$$

Figure 2.3 Schematic and Ion Flux of Platelet

was estimated from the molecular velocity of a heavy ion (Molecular weight = 129) . This value of ion molecular velocity gives reasonable agreement with experiment for the charging rate of ultrafine spherical particles and for the bipolar ion equilibrium. The ion density and the residence time within the charging section are input variables in the simulation code.

In the initial simulations the charger was based on a model used in the TSI mobility analyzer (figure 2.4). The configuration is axial flow between two concentric cylinders. The residence time used in the initial simulations were the same as for the prototype instrument used in the laboratory (essentially the same dimensions as the TSI charger). In subsequent experiments it was found necessary to redesign the charging section to a parallel plate configuration. This configuration was incorporated into the simulations. Other than the residence time the key variable was the ion density. An experimental measurement in the charger was the ion current in the charging section. Using the value of the ion current and assuming an ion velocity of 22234 cm/sec, the ion density can be calculated. In the simulations it was tacitly assumed that the ion concentration was substantially greater than the net charge acquired by the particles. This means that the ion concentration was treated as a constant.

2.4 Simulation Results

A number of simulations were carried out for both fibers and platelets. The results of some of these simulations are presented in this section. The simulation was of the operation of the Type I, prototype charger. The flow rate and physical dimensions of the charger were chosen to correspond to the prototype simulator.

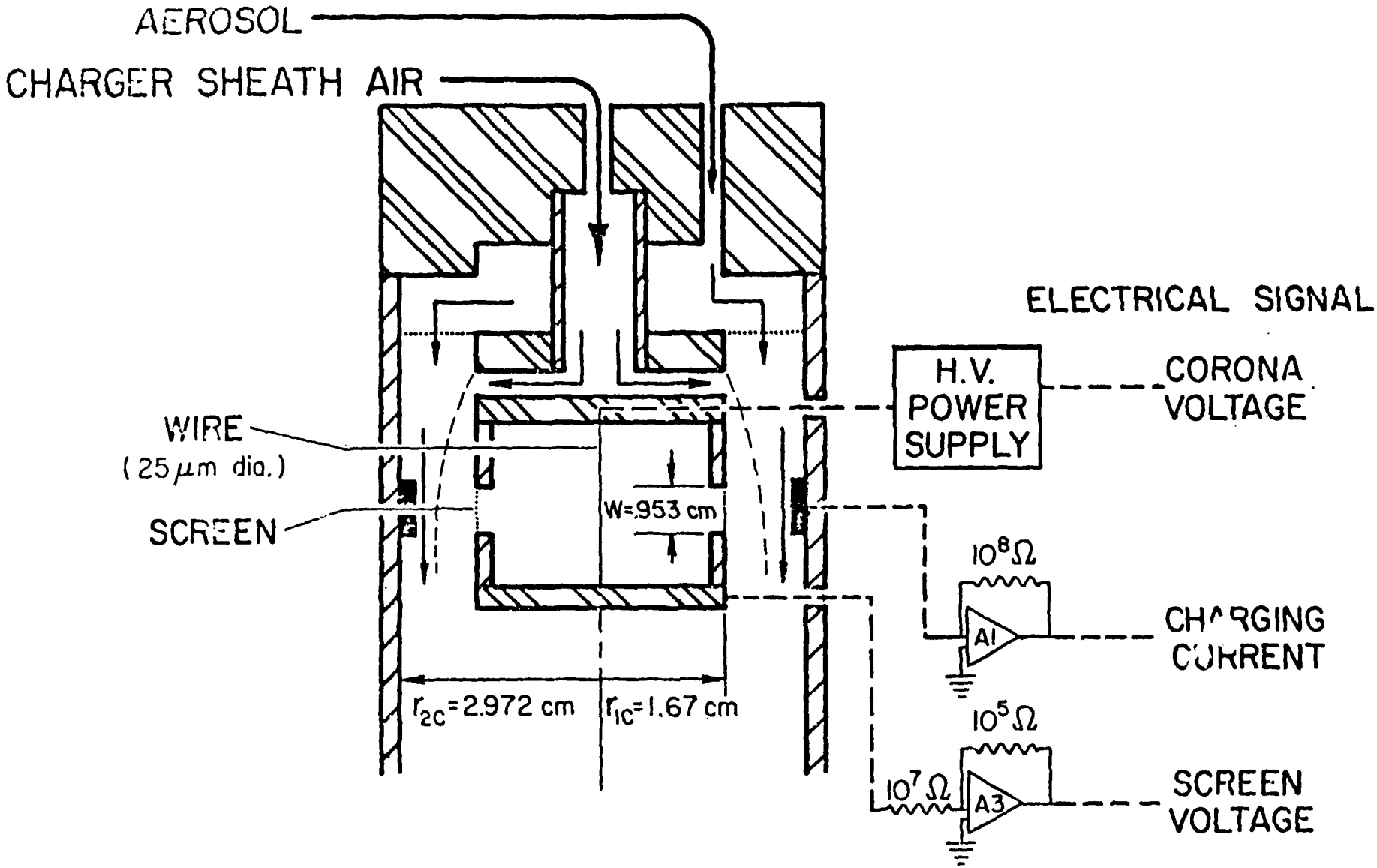

Figure 2.4 TSI Model of Charger

The loss of particles in the charger from electrostatic precipitation due to the electrical field between the bias grid and the grounded housing was neglected. It should be noted that the time in the charger was estimated at 0.271 seconds compared to typical times of 7.05 second in the precipitation section after the charger. In typical simulations the fiber diameter (or platelet thickness) was fixed and the aspect ratio and N_0t varied.

Typical results of the simulations are presented as three dimensional plots with the number of charges acquired plotted as a function of aspect ratio and N_0t. For contrast the number of charges acquired are usually compared with spherical particles of the same volume or area. In this section there are six simulations with fibers and ten simulations with platelets. The summary of the simulations are listed in Table 2.1.

In the simulations of the charging of fibers we examined several points : are the fibers more heavily charged than spherical particles of the same volume, is the difference affected by the fiber diameter (i.e. the effect of the image term increases with fiber diameters), and what would the effect be if the fibers were very long. In typical experiments with asbestos or other very thin mineral fibers, the aspect ratioes were in the range of $10 - 80$. However, the carbon fibers were much longer and their aspect ratioes ranged up to 1000. The smaller fibers are simulated in figure 2.5-2.7 and the larger fibers in figures 2.8-2.10.

For the smaller fibers the number of acquired charges are plotted for three aspect ratioes 8, 20, and 60. The number of charges increase with the aspect ratio. For the thinnest fibers, where the image term is most important. The

TABLE 2.1 Summary of Simulation Conditions For Non-Spherical Particles

FIGURE	SHAPE	DIAMETER	COMPARISON
2.5	Fiber	0.01	Equal Volume
2.6	Fiber	0.03	Equal Volume
2.7	Fiber	0.05	Equal Volume
2.8	Fiber	0.05	Equal Volume(long fiber)
2.9	Fiber	0.10	Equal Volume(long fiber)
2.10	Fiber	0.30	Equal Volume(long fiber)
FIGURE	SHAPE	ASPECT RATIO	COMPARISON
2.11	Flake	0.01	Equal Volume
2.12	Flake	0.05	Equal Volume
2.13	Flake	0.10	Equal Volume
2.14	Flake	0.01	Equal Surface
2.15	Flake	0.05	Equal Surface
2.16	Flake	0.10	Equal Surface
2.17	Flake	0.01	Effect of Image
2.18	Flake	0.05	Effect of Image
2.19	Flake	0.05	Effect of Image(large D)
2.20	Flake	0.05	Equal Volume of Fiber

fibers are much more heavily charged than the spherical particles of the same volume. As the particle diameter increases, the image term becomes less important. However the Coulombic repulsion increases more rapidly for the thin fiber than for the thicker sphere. The result is an inversion for the shorter fibers, where the spherical particles actually acquire charges more rapidly. It should be noted that in this case one is talking only about 2 or 3 charges. The simulations strongly suggest that fibers are more heavily charged than spherical particles of the same volume. They suggest that the greater the aspect ratio the more significant this effect. Finally, there is a significant difference in the number of charges only for the longer fibers. They suggest that separation of long fibers can be acomplished using electrostatic classification, but that the separation will become more difficult as the fiber diameter increases, and the aspect ratio approaches that of a sphere.

The longer fibers were thicker, but had aspect ratioes of 200, 600, and 1000. The data for these simulations are presented in figures 2.8-2.10. First the fibers had more than five times the charges as the spherical particles of equal volume. The number of charges increased rapidly as the aspect ratio increased. These simulations suggest that increasing the ion density has more effect when the fibers are longer. We believe that the explanation as to why there is less of an effect as the fibers become shorter and thicker, is that eventually an effective saturation charge is reached where it is difficult to add additional charges. The flux decreases to the point that the charge on the particle remains almost constant after the initial charging. In this case the controlling factor is the repulsion, which increases exponentially with the inverse of the fiber or

spherical diameter. For fibers this diameter is smaller so that repulsion may be sufficiently great that it more than compensates for the greater surface area of the fibers. However, the main conclusions which can be drawn from these studies is that the longer the aspect ratio, the more charges the fibers acquire and that separation of long fibers is very possible with electrostatic forces.

The simulations for the flake differed. The aspect ratio (plate thickness to plate diameter) was fixed and the ion current and flake diameter were the variable parameters. The flakes were small with a diameter ranging upwards to $0.5\mu m$ and the thickness varying from $0.05\mu m$ to $0.005\mu m$. From the figures 2.11-2.13 it is clear that the flakes have aquired a signinficntly higher charge than spherical particles of equivalent volume. As the platelets become thicker, the effect is less marked. It is interesting to note that the thickness has little influence on the total charge that the platelets obtain. This is due to the model where the image term does not depend on platelet thickness and the surface area of the flake is not greatly affected.

In figures 2.14-2.16 the charge for the flakes are compared with spherical particles of the same area. The number of charges does not change significantly with plate thickness. The explanation is the same as above. One notices that the number of charges does not change greatly as the $N_0 t$ increases. This implies that the charging rate is controlled by the repulsion due to the Coulombic potential. The surprising result is that the aquisition of charge is essentially that of a sphere of equal area.

In figures 2.17-2.19 the effect of image term is examined. The calculation

is performed on the same model with the same Coulombic potential between charge and particle. For small particles the image term plays an important role, as the particle aquires about 50% more charges when the image term is included. For larger particles the charge increase is not so large although the number of charge is greater.

In figure 2.20 a comparison is made between the flake and the fiber. The volume of the two particles are the same. The diameter is that of the plate. The fiber diameter is adjusted so that the volume of the particle is the same. In this case the ratio of fiber length to fiber diameter is the same as the ratio of flake diameter to flake thickness. The results are striking, for the smaller volume particles the fiber aquires a much higher number of charges. Surprizingly as the particles become larger, eventually the flake aquires a higher charge. This is an example of the much greater importance of the image term for fibers than for platelets or flakes.

In conclusion the simulations indicate that non-spherical particles aquired more charges than spherical particles of the same volume. Since the drag may be less as well, it is easy to visualizes circumstances in which particles may be charged to obtain greater separation of fibers in an electrostatic precipitator.

Text continues on page 39

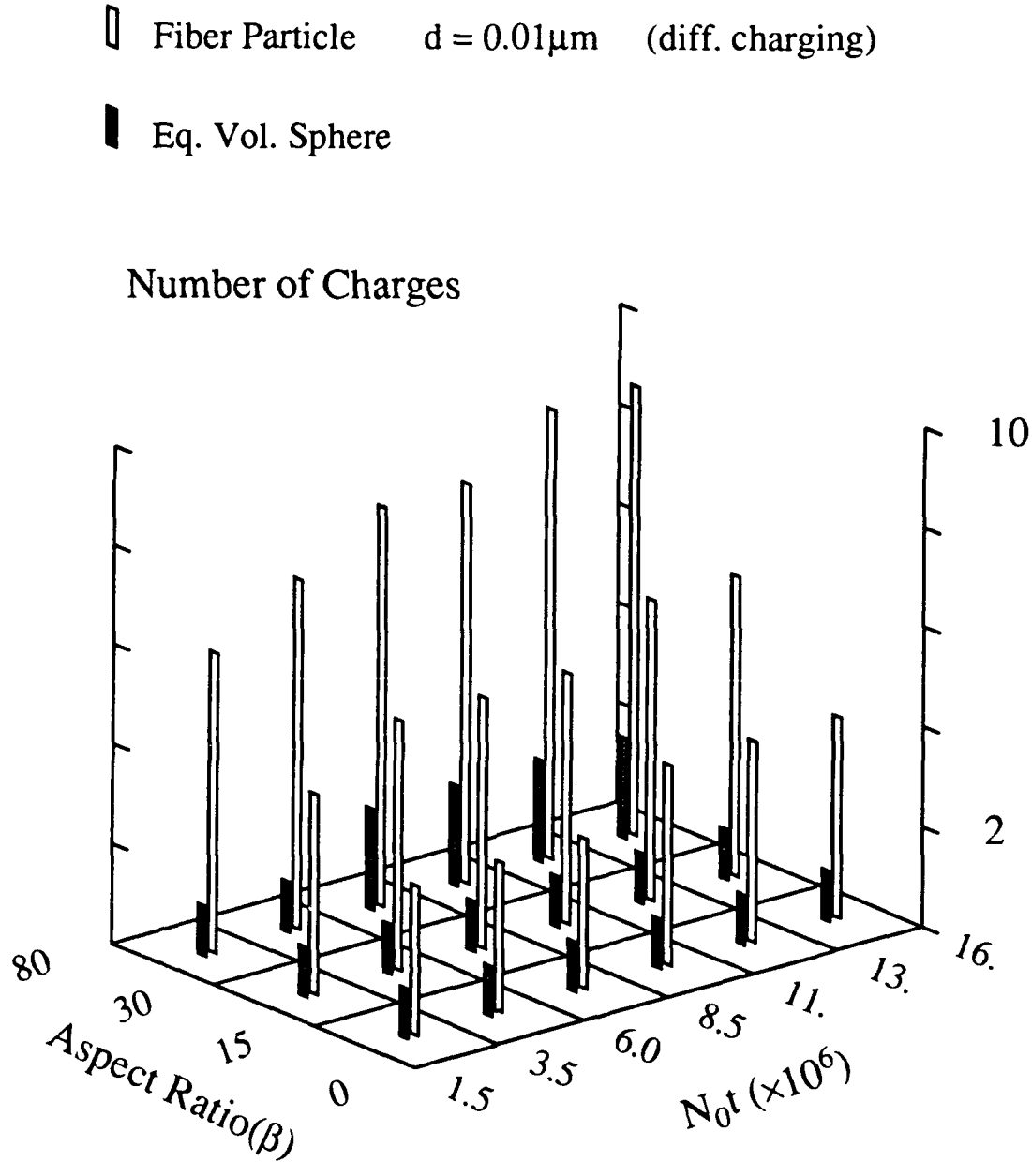

Figure 2.5 Comparison of charge number between 0.01 micron diameter fiber and equal volume sphere

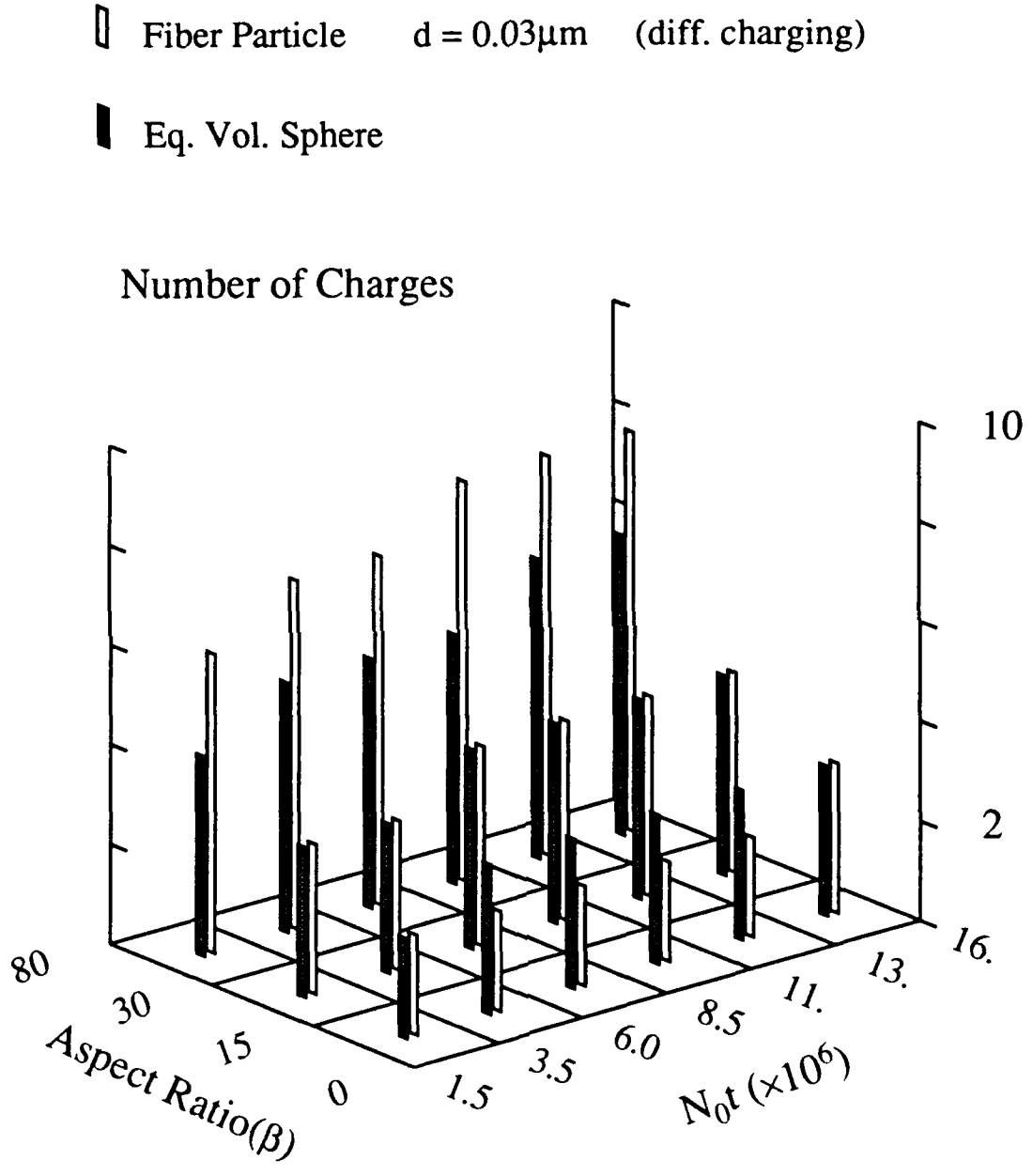

Figure 2.6 Comparison of charge number between 0.03 micron diameter fiber and equal volume sphere

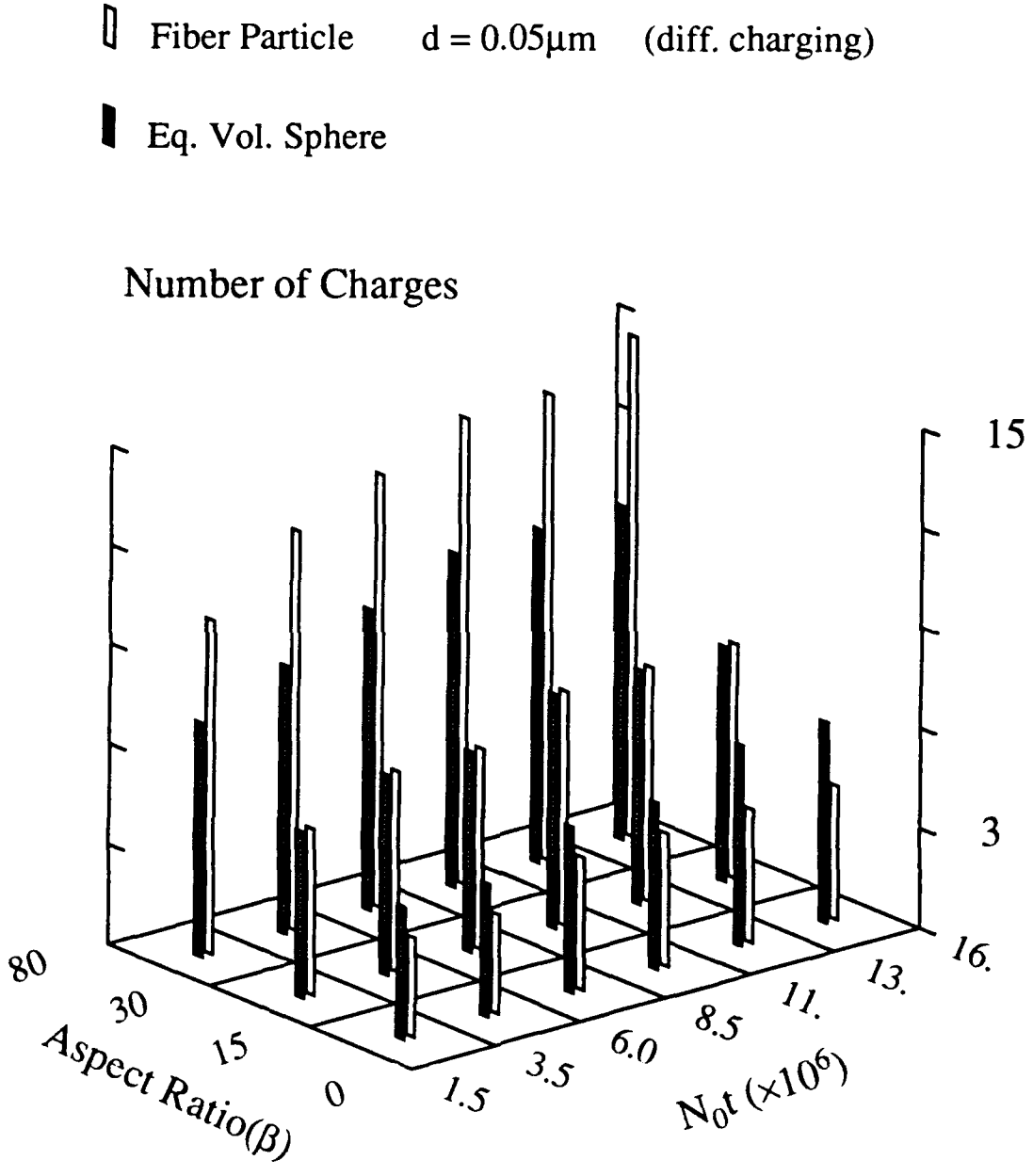

Figure 2.7 Comparison of charge number between 0.05 micron diameter fiber and equal volume sphere

Fiber Particle d = 0.05μm (diff. charging)

Eq. Vol. Sphere

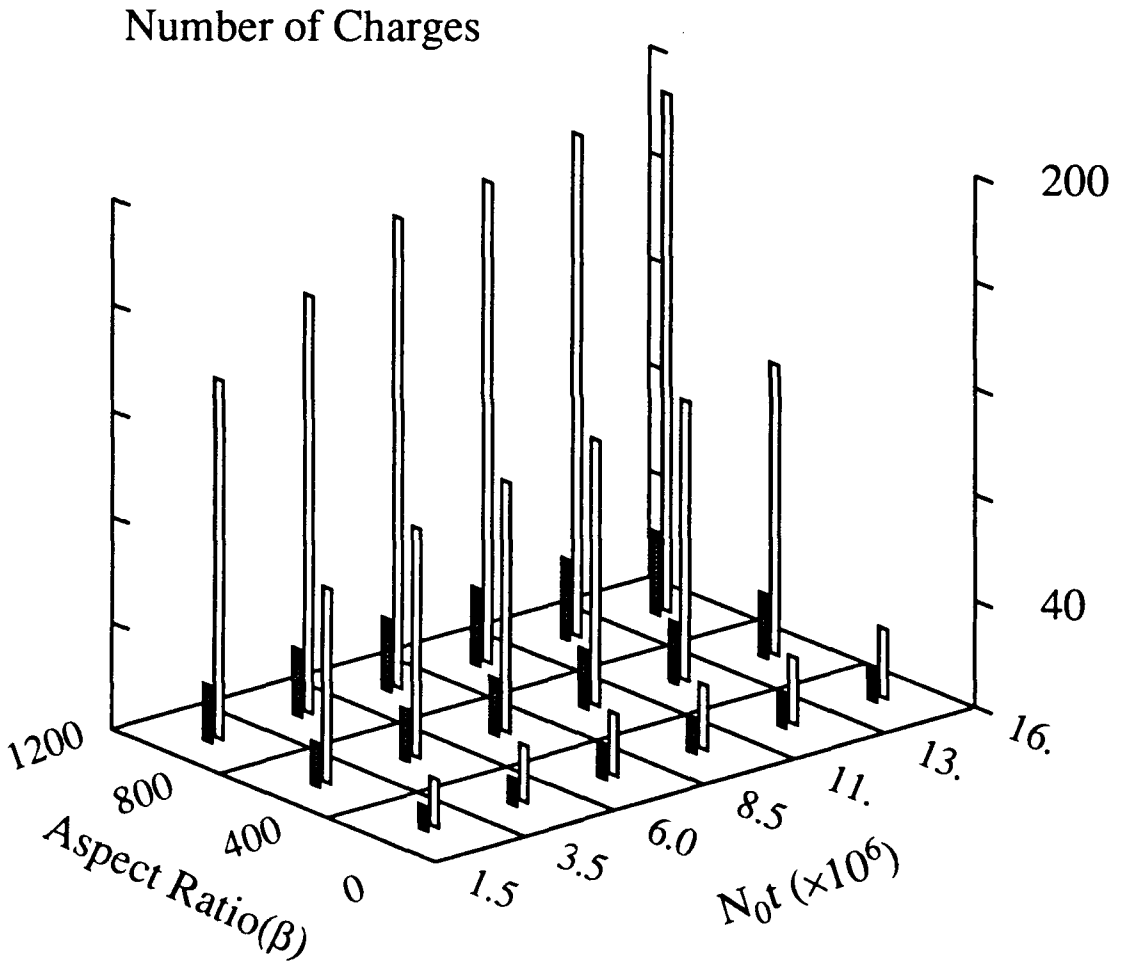

Figure 2.8 Comparison of charge number between 0.05 micron diameter fiber and equal volume sphere

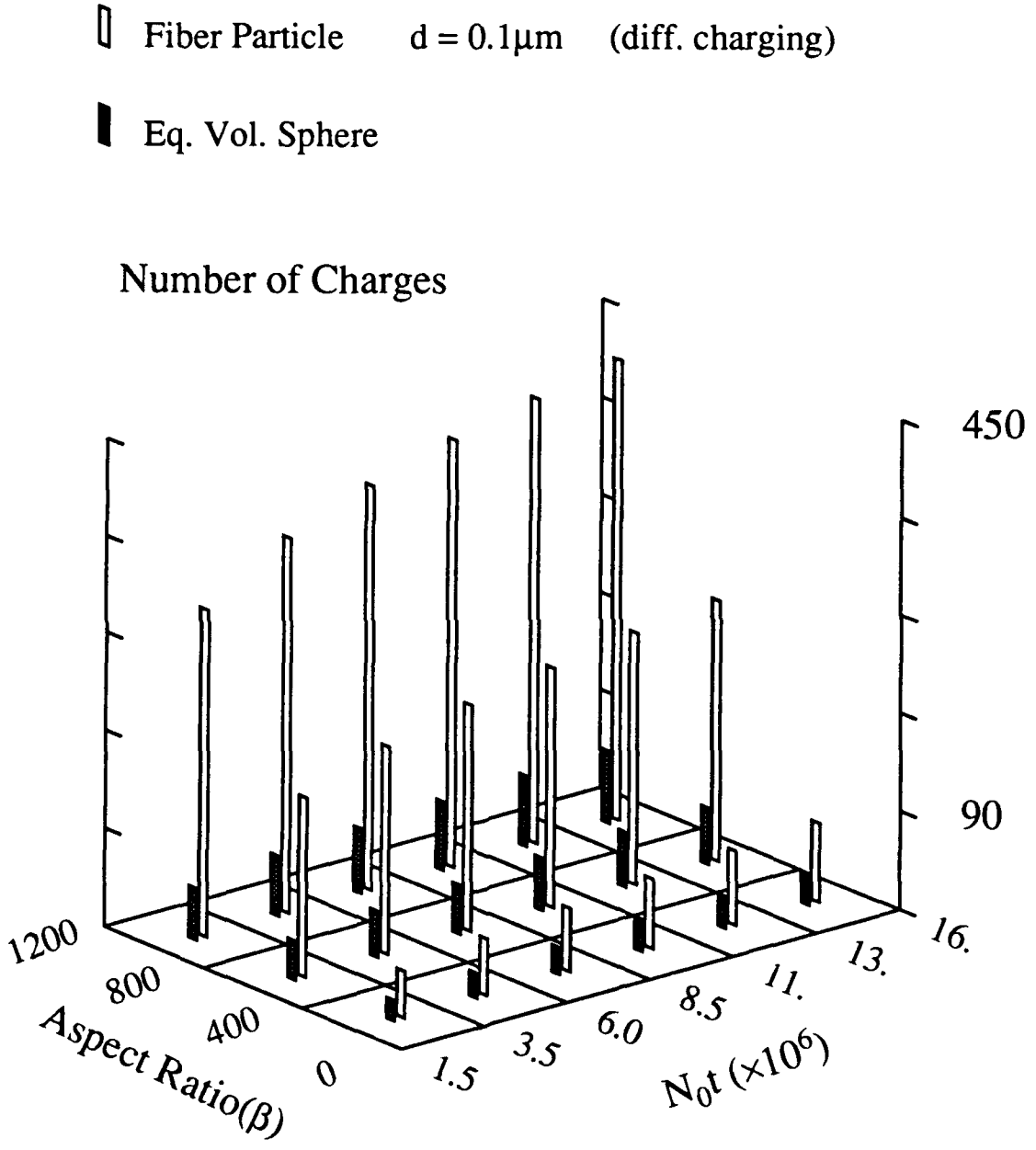

Figure 2.9 Comparison of charge number between 0.1 micron diameter fiber and equal volume sphere

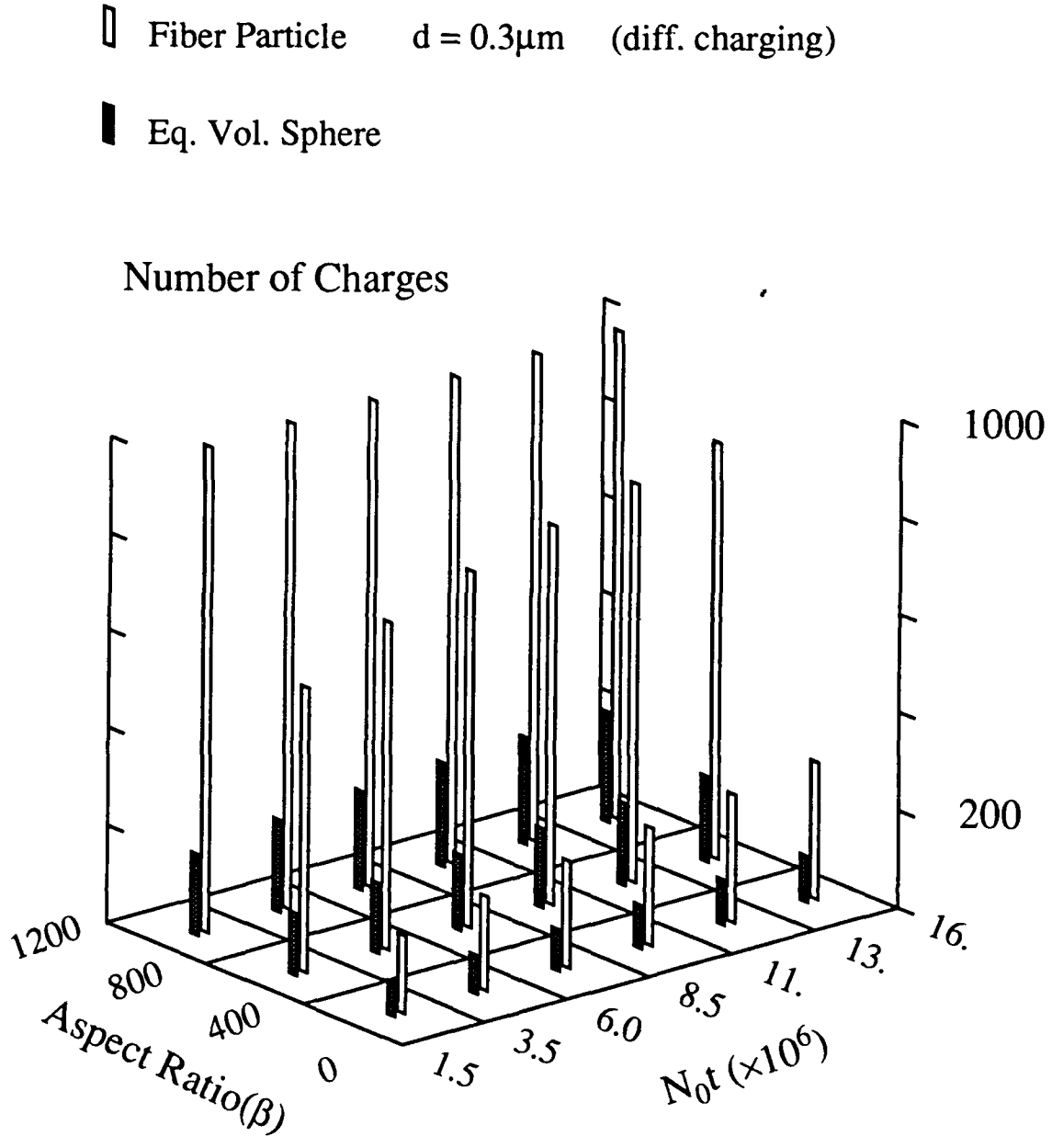

Figure 2.10 Comparison of charge number between 0.3 micron diameter fiber and equal volume sphere

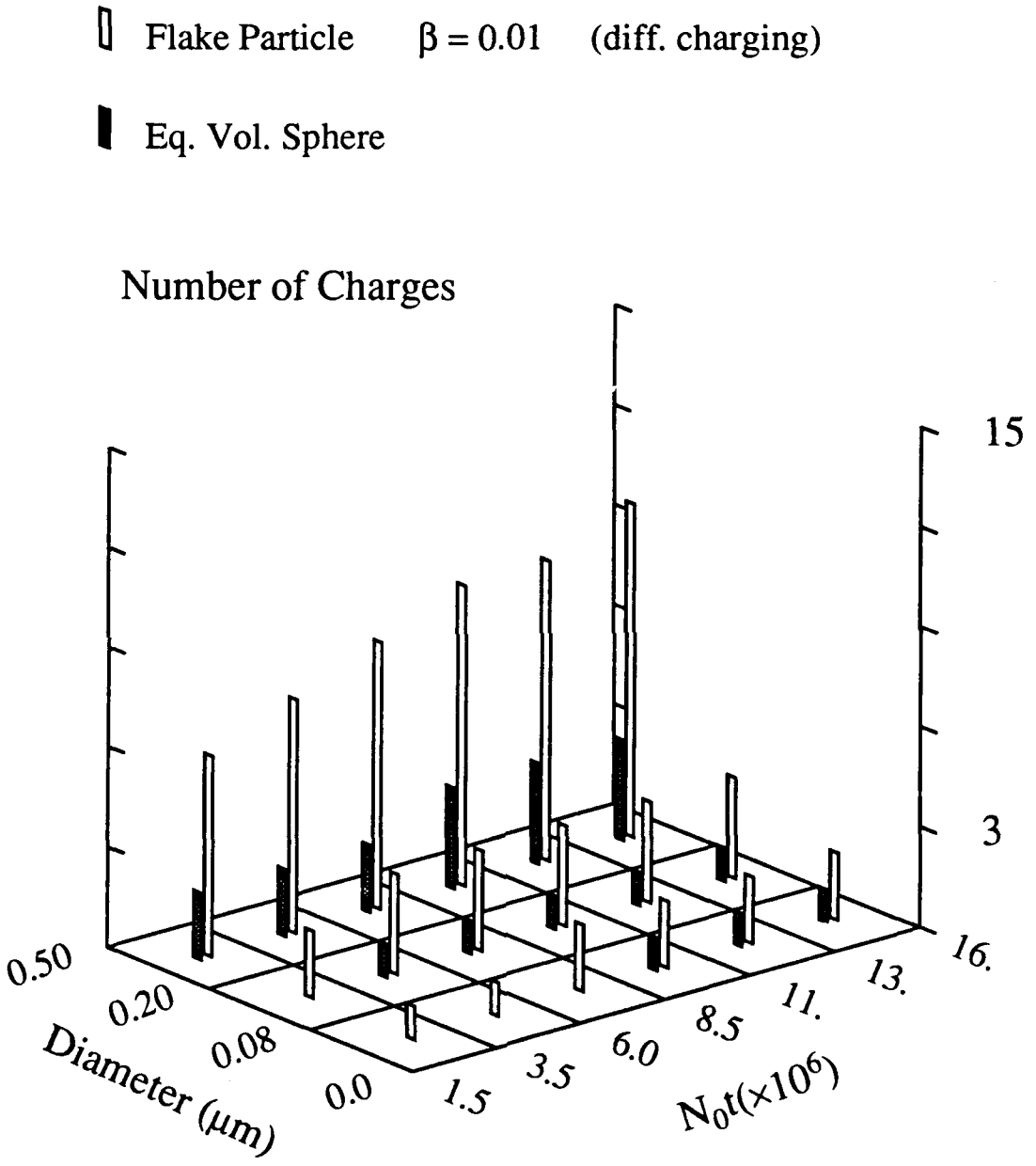

Figure 2.11 Comparison of charge number between 0.01 aspect ratio flake and equal volume sphere

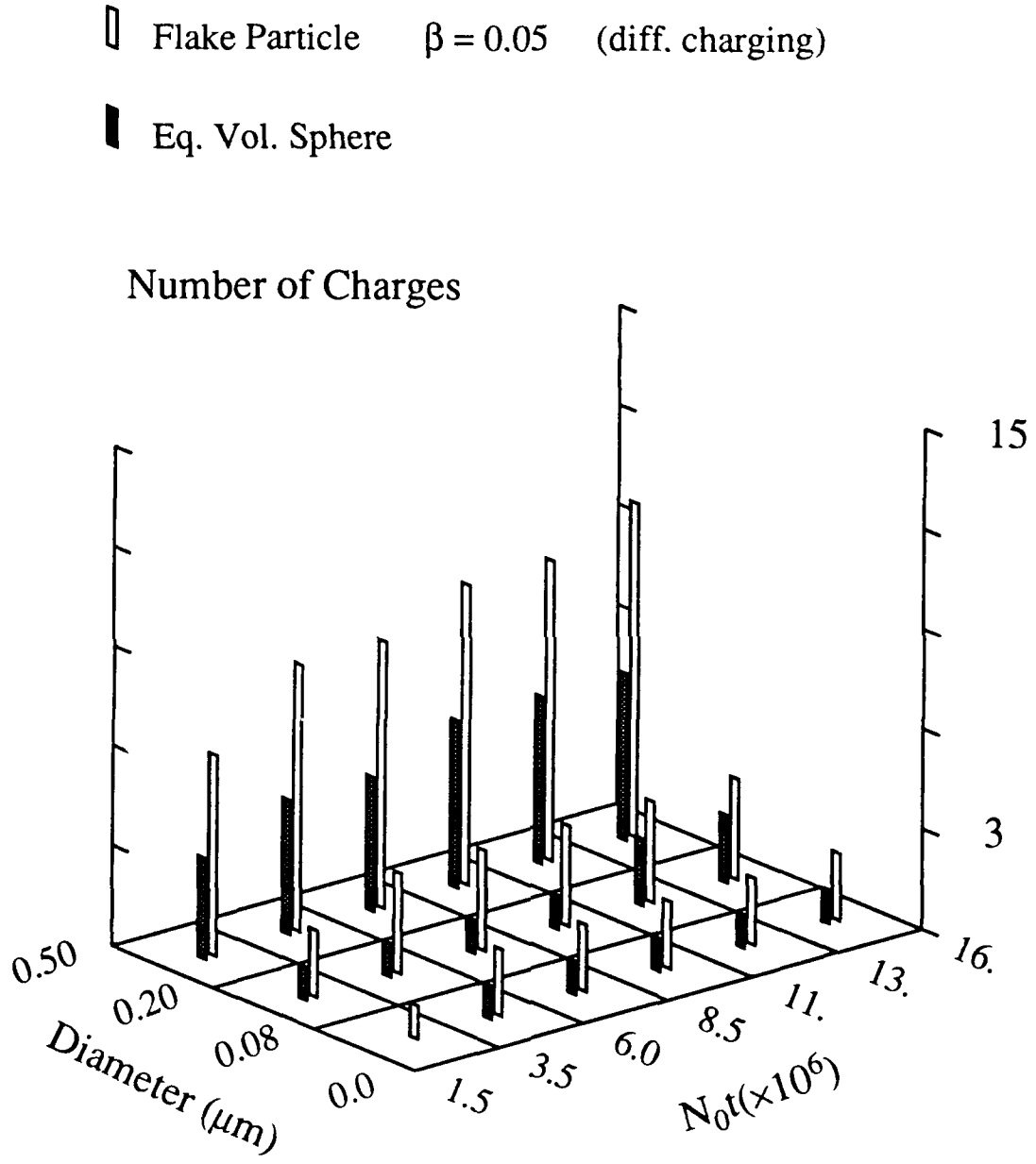

Figure 2.12 Comparison of charge number between 0.05 aspect ratio flake and equal volume sphere

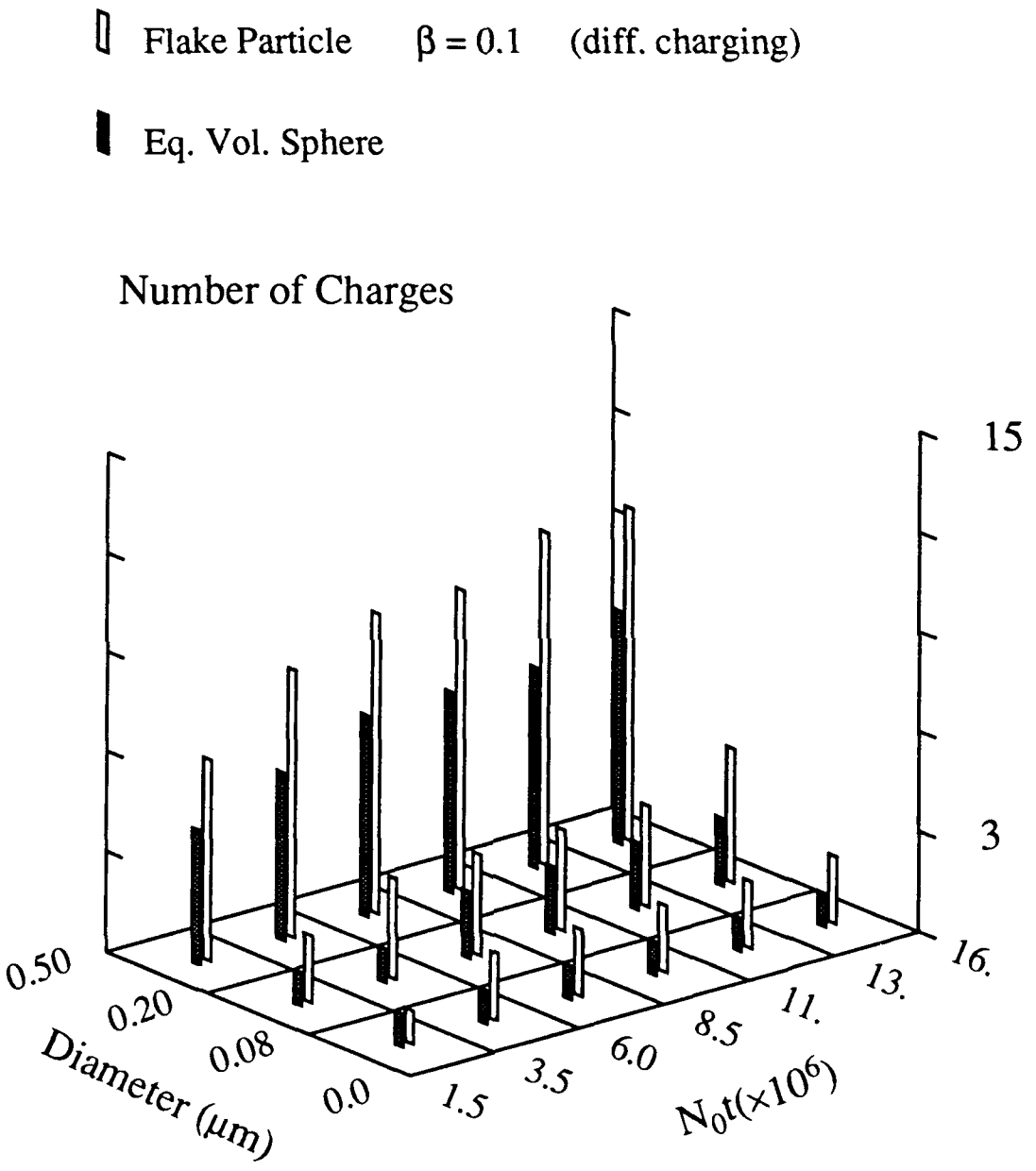

Figure 2.13 Comparison of charge number between 0.1 aspect ratio flake and equal volume sphere

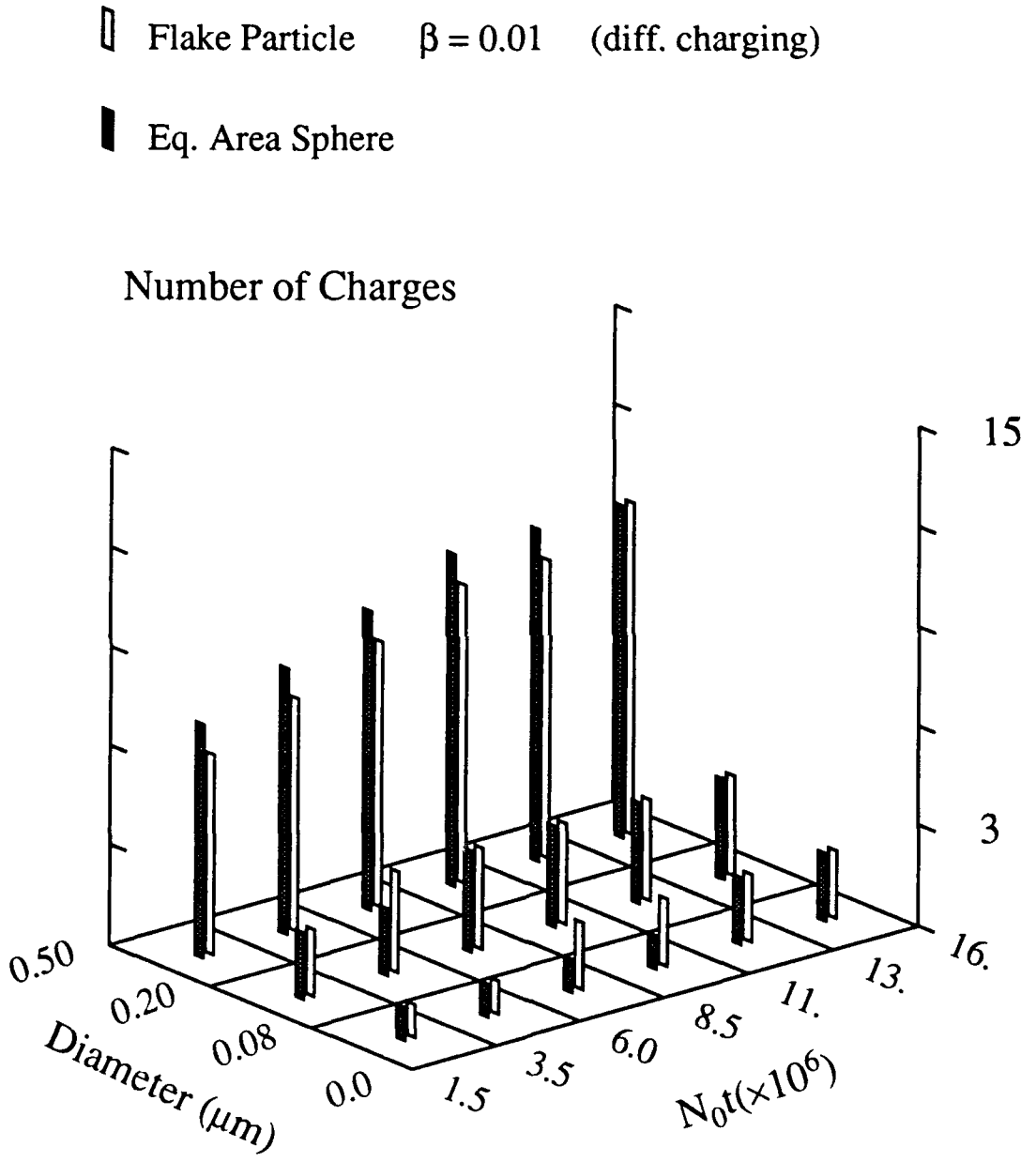

Figure 2.14 Comparison of charge number between 0.01 aspect ratio flake and equal area sphere

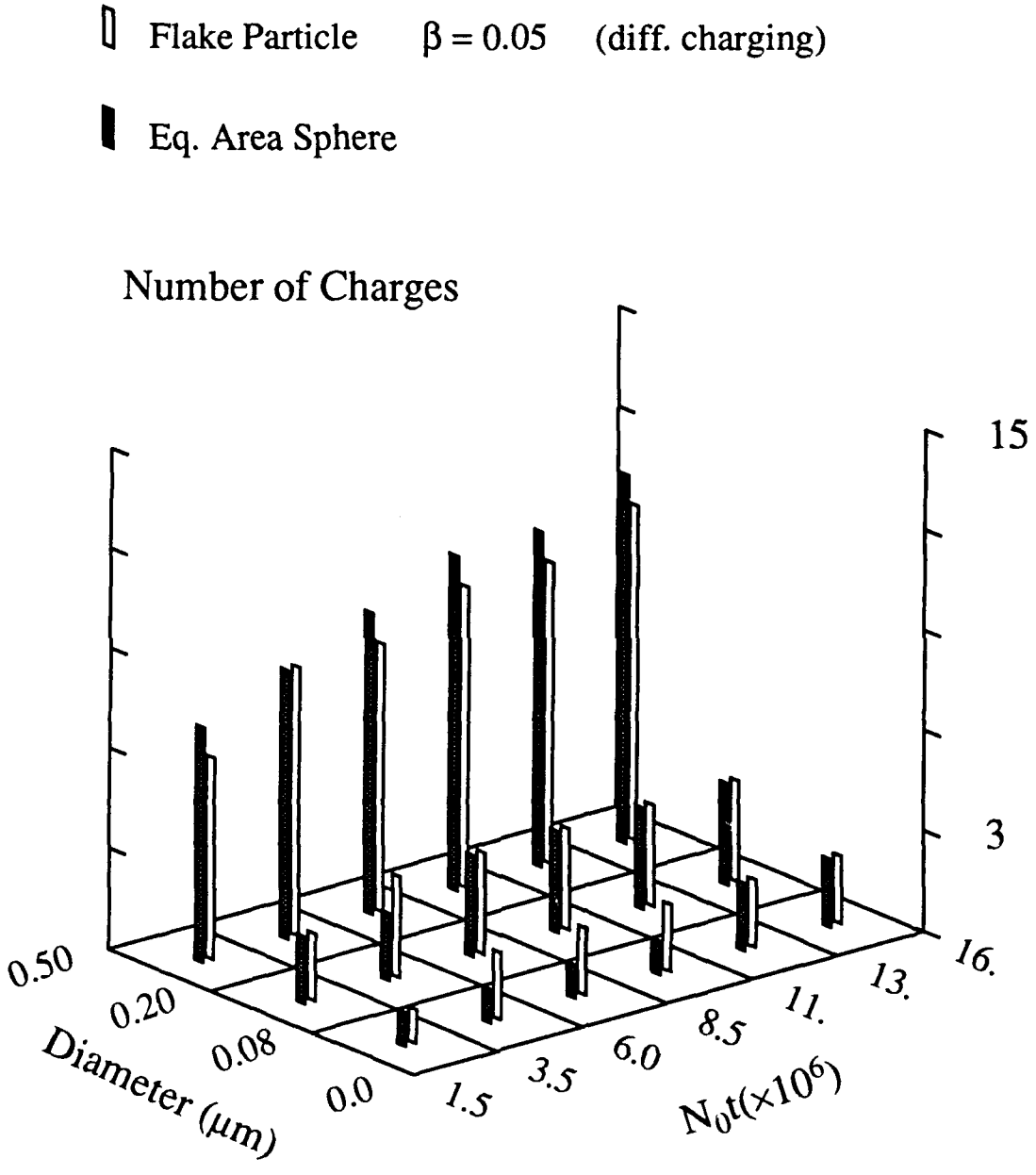

Figure 2.15 Comparison of charge number between 0.05 aspect ratio flake and equal area sphere

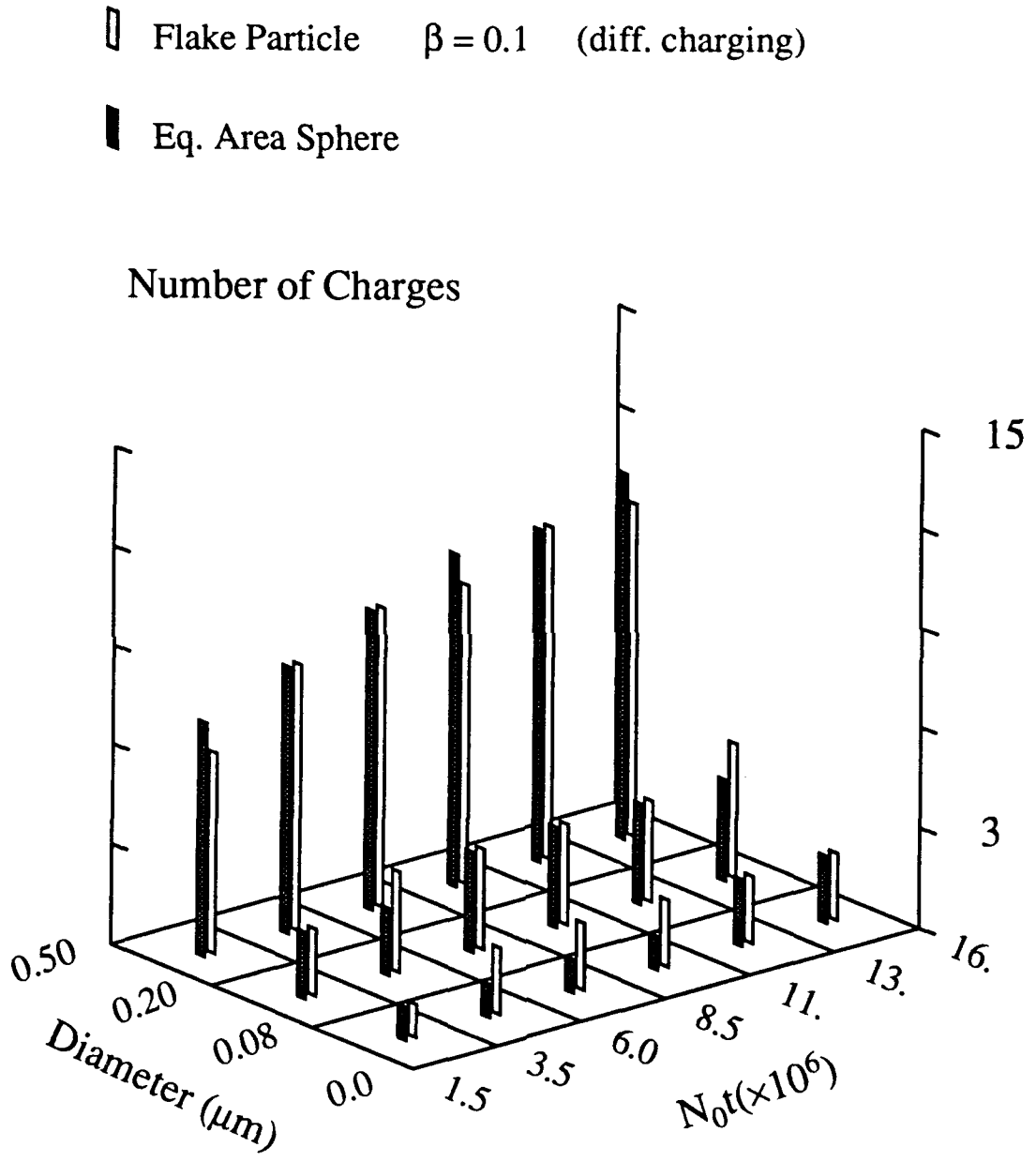

Figure 2.16 Comparison of charge number between 0.1 aspect ratio flake and equal area sphere

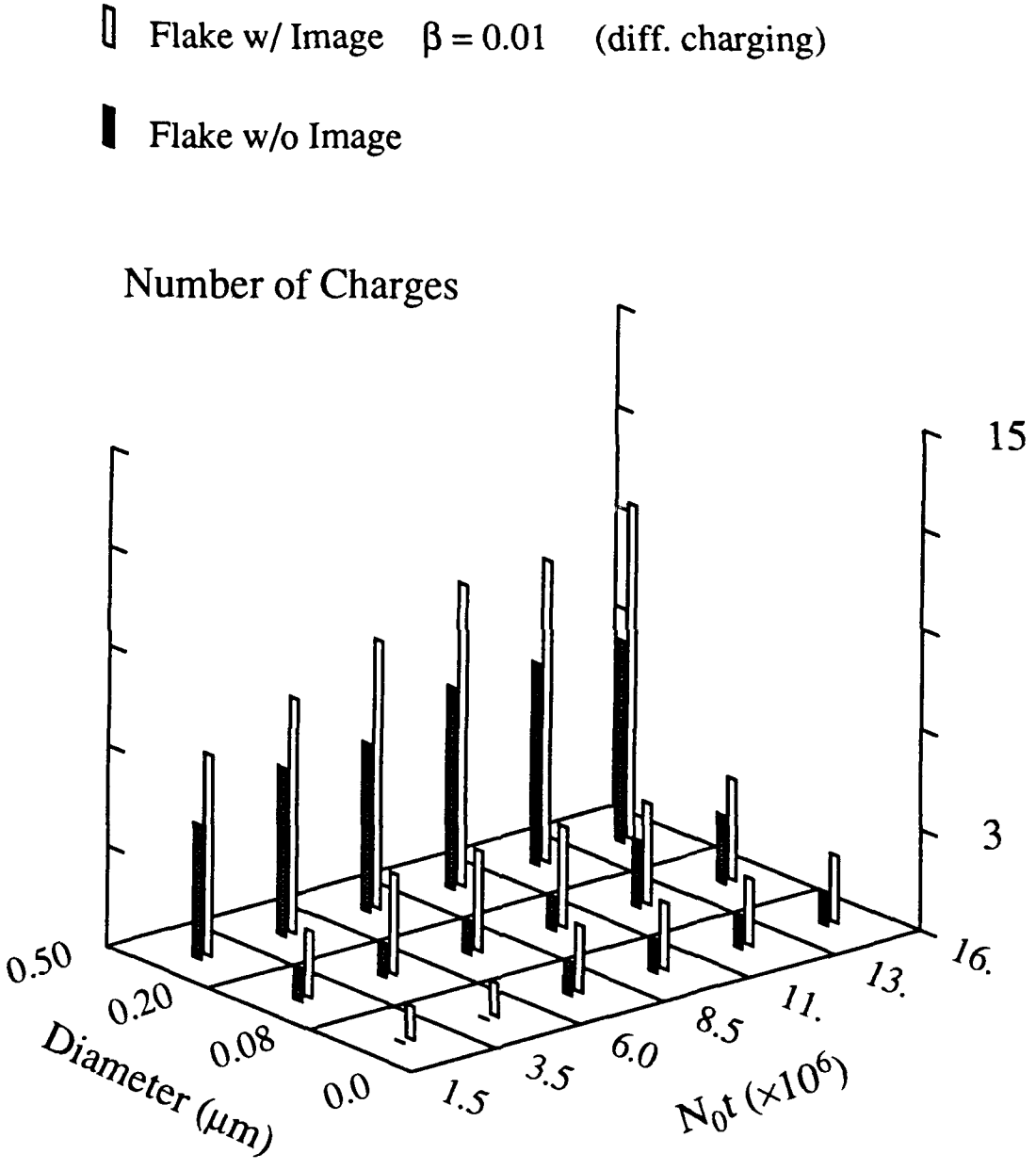

Figure 2.17 Effect of image term on flake charging

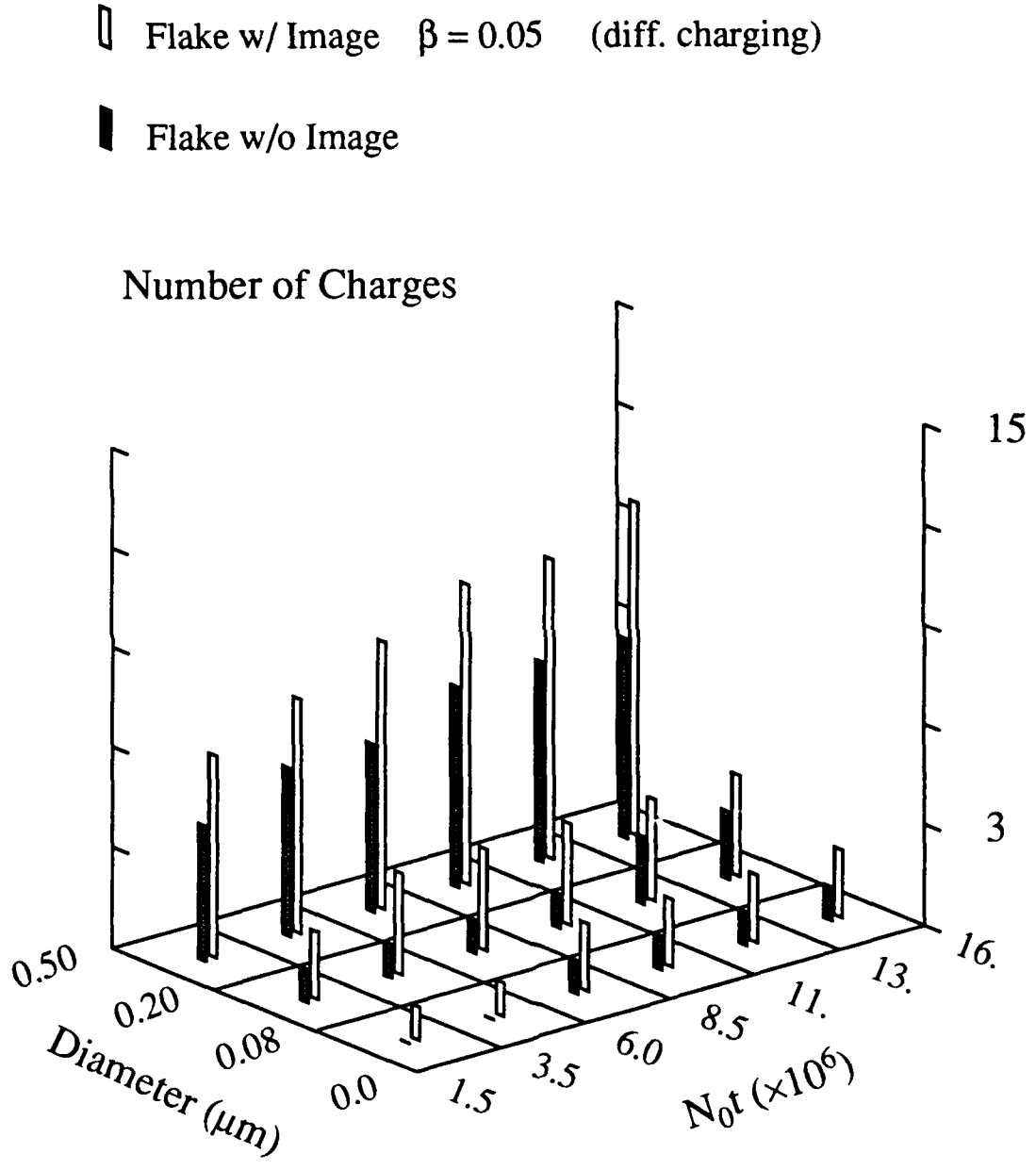

Figure 2.18 Effect of image term on flake charging

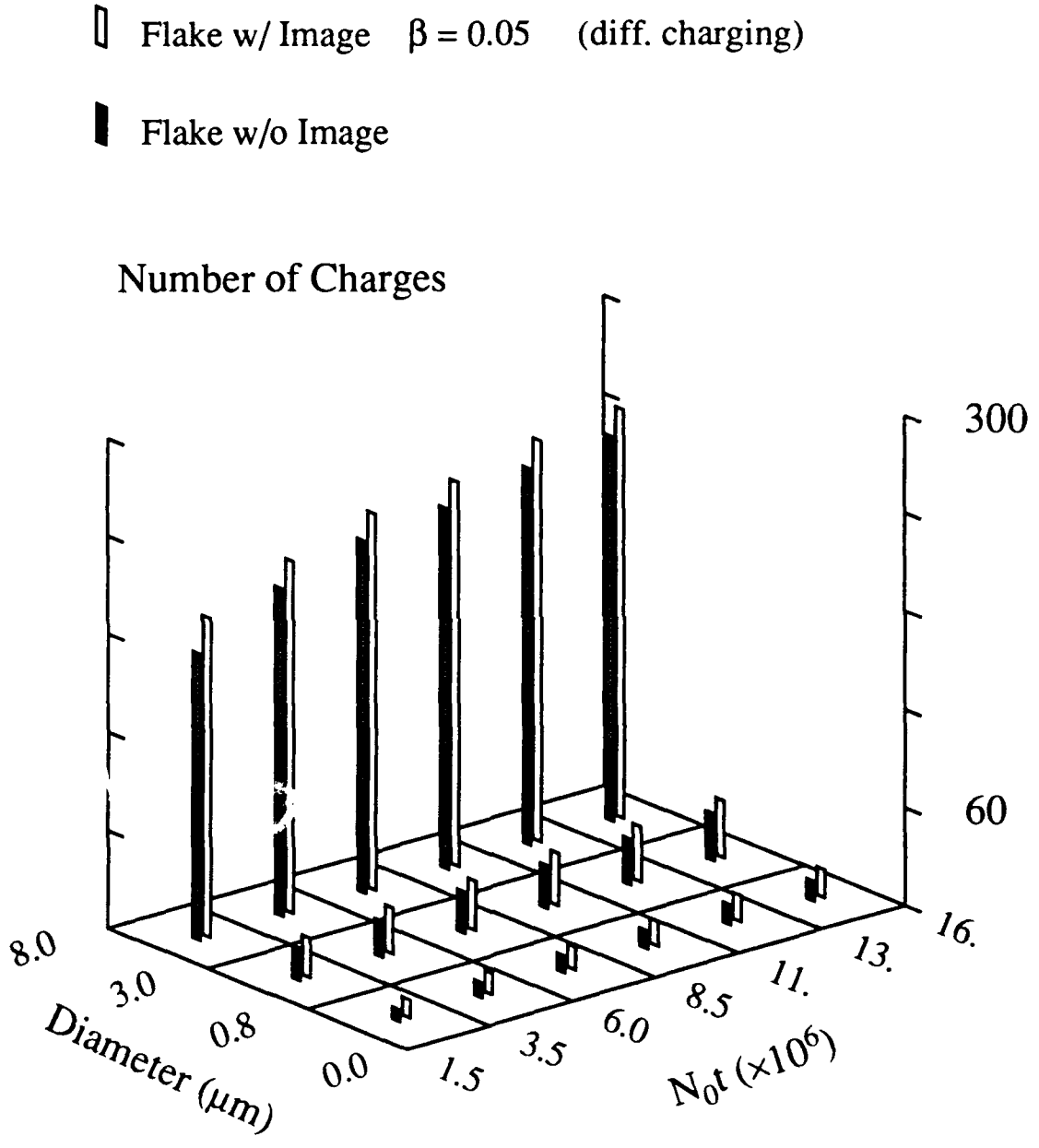

Figure 2.19 Effect of image term on flake charging

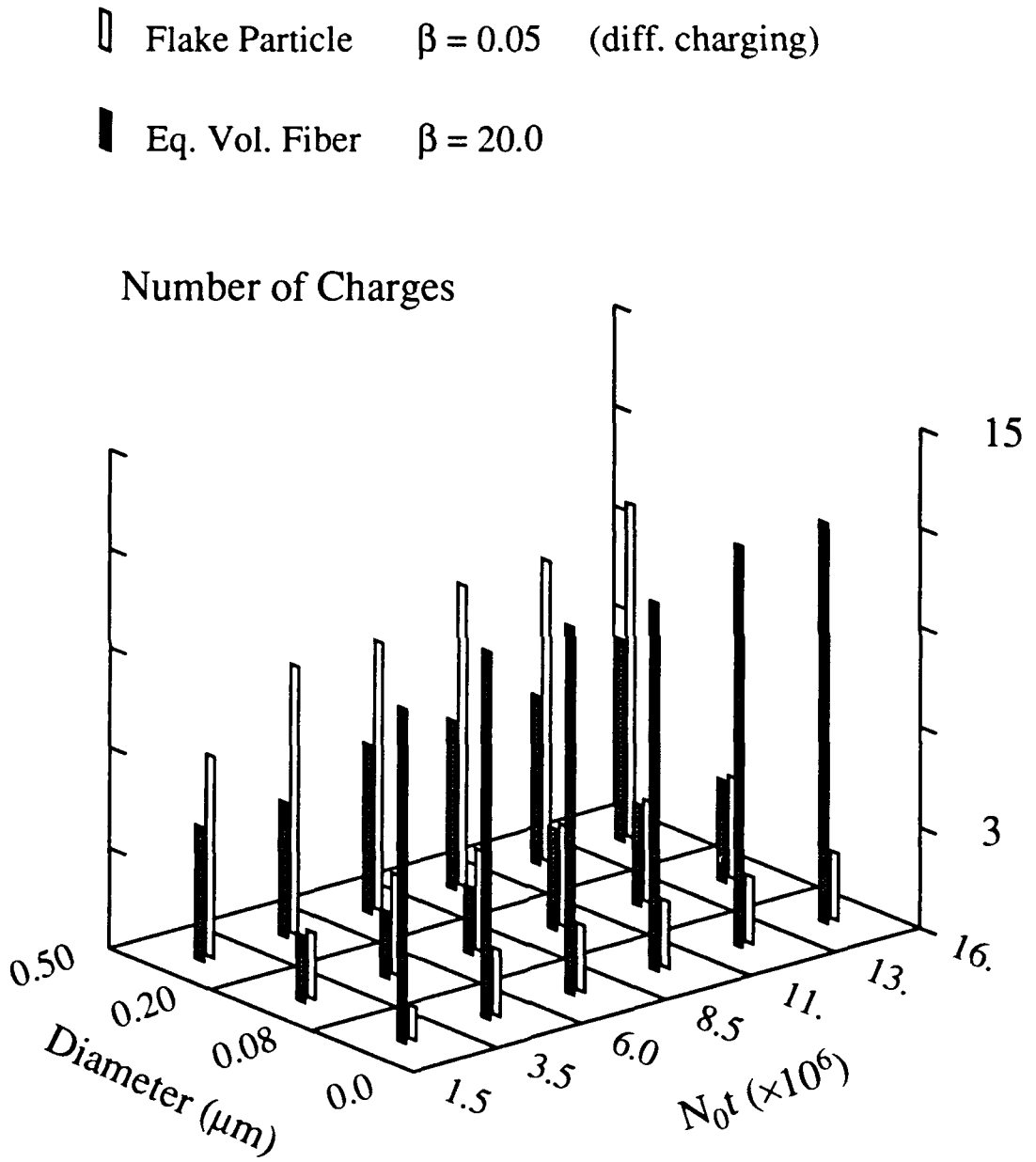

Figure 2.20 Comparison of charge number between the same volume flake and fiber particles

3. EXPERIMENTAL INVESTIGATION OF POWDERS

Two types of fibers were used in the preliminary exeriments - carbon fibers and iron fibers. The fibers were entrained in an air stream after agitation in a blender.

The fibers (either carbon or iron) tend to be hygroscopic, so that in time they adsorb water vapor. This creates adhesive forces between the fibers making them more difficult to disperse. This effect can be minimized by heating the fibrous powder before dispersion in air. It was standard procedure to heat the fiber material for 24 hours at $80 - 90°C$. before usage. This resulted in the production of large numbers of individual fibers. It was found that heating the fibers before their usage was essential if individual fibers were to be produced.

One set of experiment was carried out using Carbon flakes.

3.1 Experimental Apparatus

A schematic diagram of the apparatus is shown in figure 3.1. The fiber and flake aerosol have a tendency to clump. We were able to disperse them successfully using a two stage system. The fibers are first dispersed into a common food blender and then aspirated into a high speed pneumatic ejector where they were further separated. Because of the intense mechanical action triboeletric charges on the fibers were significant. A Krypton 85 source sealed in a shielded tube was used to produce bipolar ions to neutralize the fibers. A coarse grid removed very large aggregates before the fibers enter the charger. The aerosol flowed vertically down between a parallel plate electrostatic precipitator. One plate was maintained at a high positive voltage and the other plate was grounded. A

final $47mm$ filter collected particles penetrating the precipitator. The flow was controlled by a vacuum pump and a flow meter.

The two plate electrodes from the precipitator could be removed to examine the deposited particles.

Design of Charger

Three different charger designs were examined. Schematic diagrams of the chargers are shown in figures 3.2 , 3.3, and 3.4. The first design was a modification of the unipolar charger used in charger used in the TSI Model 3030 Electrical aerosol analyzer. It has the configuration of annular flow parallel to the charging wire. The major features of the design are

(1) The corona wire which is maintained at a high electrical potential. Much of the preliminary operations were carried out at voltages below the point where there was a corona discharge (i.e. $3000V$) . ,

(2) The bias screen voltage which is maintained at a constant voltage of ($50 - 400V$). Depending on the bias voltage and the grid size of the bias screen , it should be possible to produce a unipolarly charged stream of ions. However there is clear indication that for lower bias voltages , that the net flux of unipolarly charged ions can drop off sharply. The effect of grid screen size has not been discussed in the literature , and experiments in this area are now in progress.

(3) The brass foil at the end of the charging section is used to determine the ion current from the bias screen to the walls of the charger. This provides a direct measurement of the ion concentration within the charger.

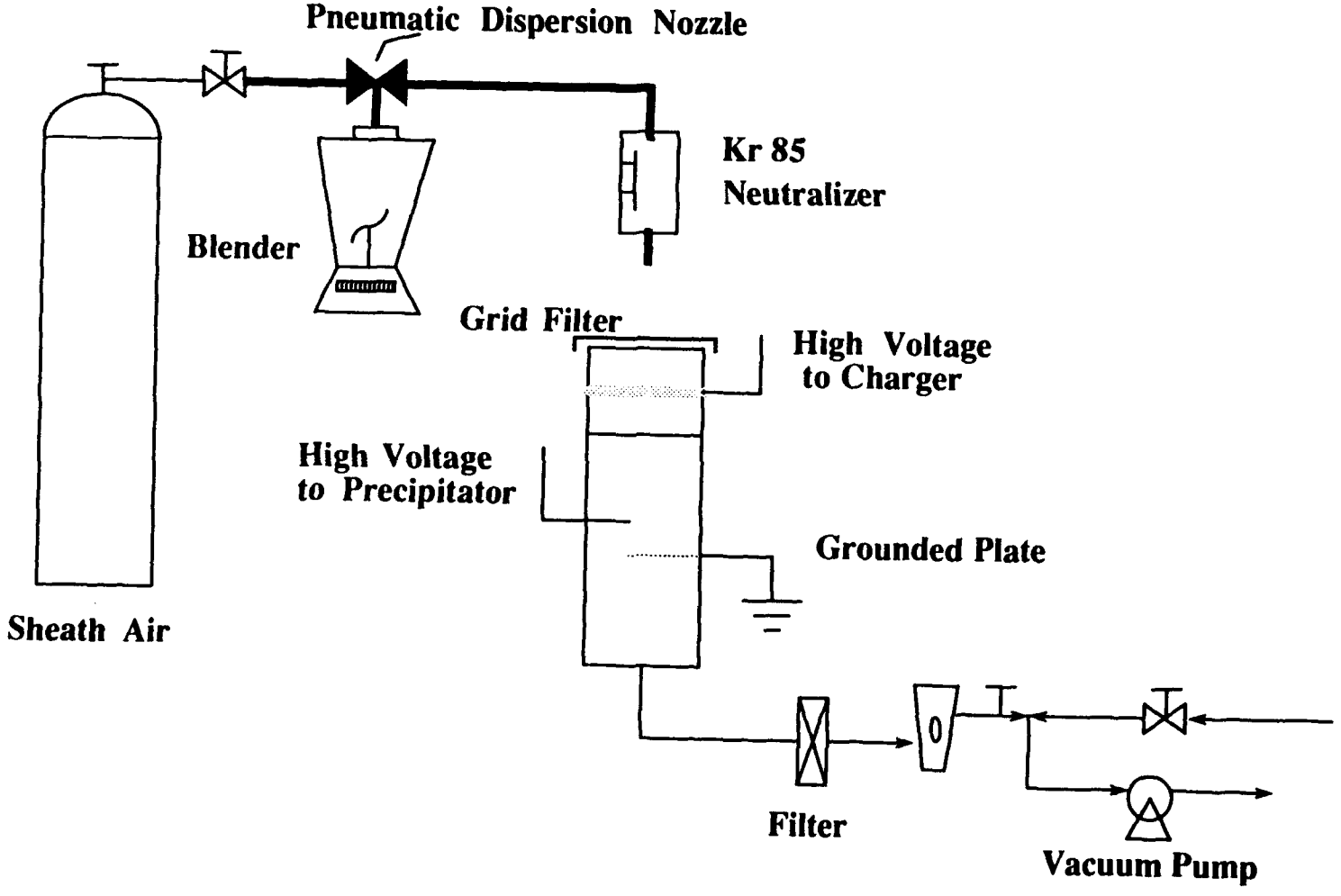

Figure 3.1 Schematic Diagram of Apparatus

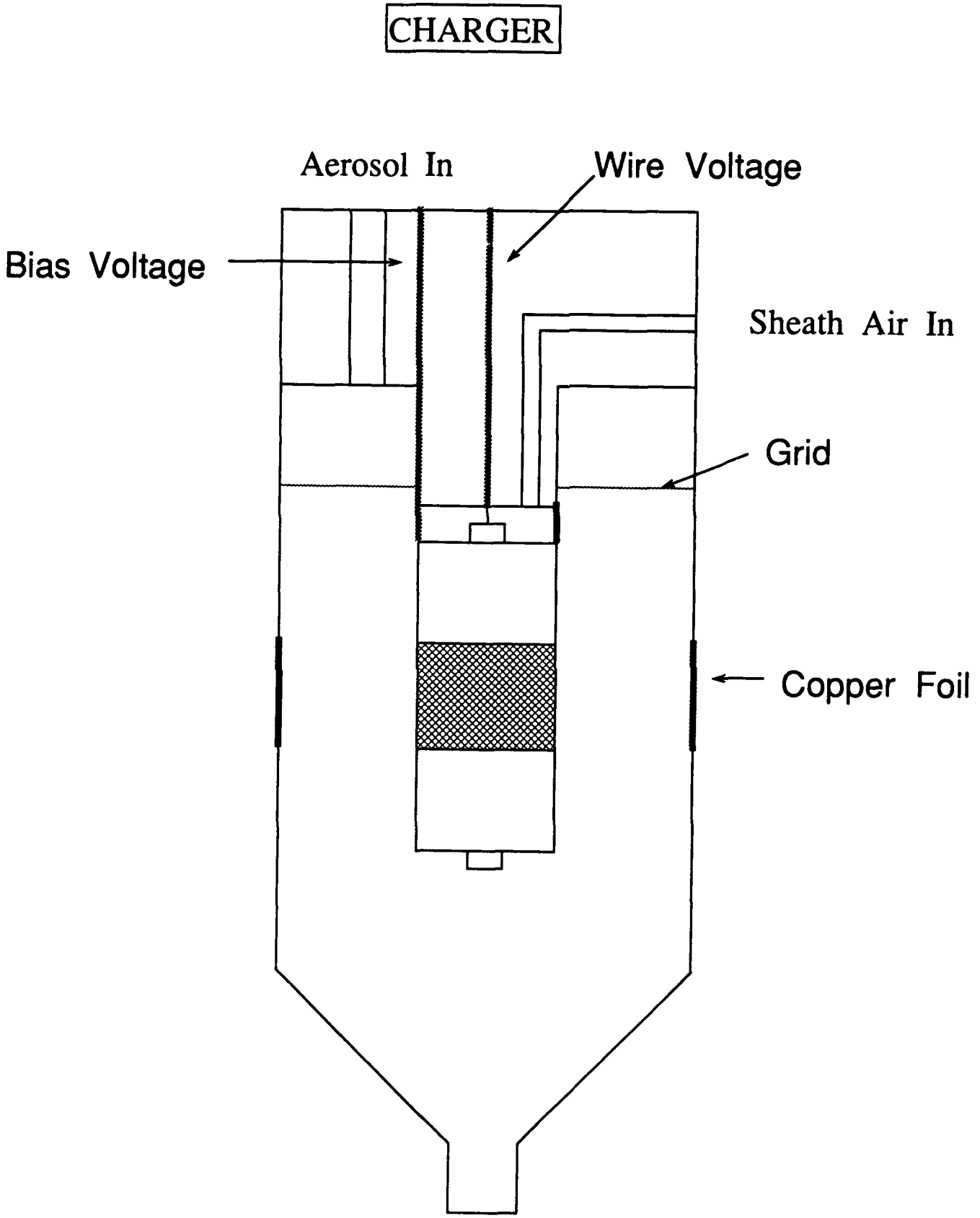

Figure 3.2 Modified Charger

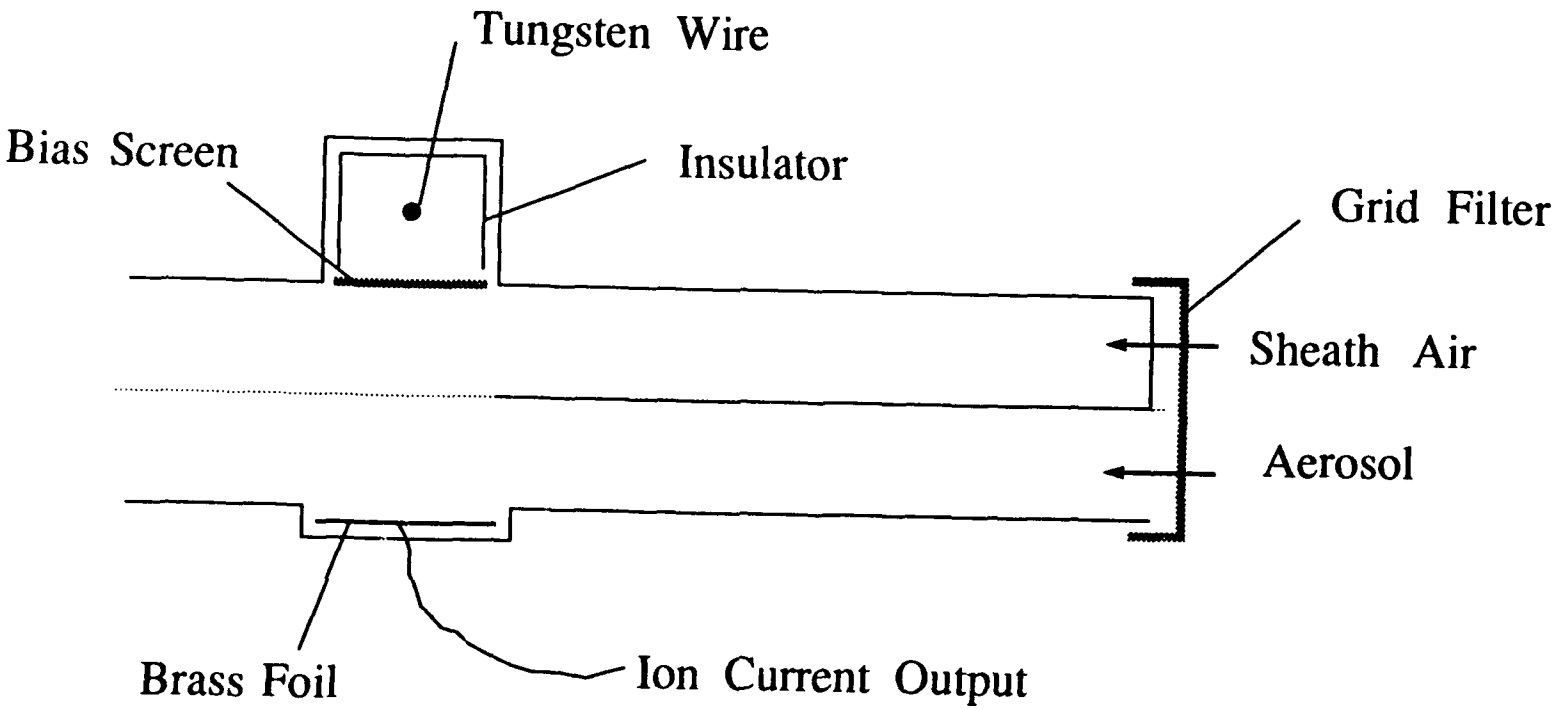

Figure 3.3 Parallel Plate Charger Model with One Wire

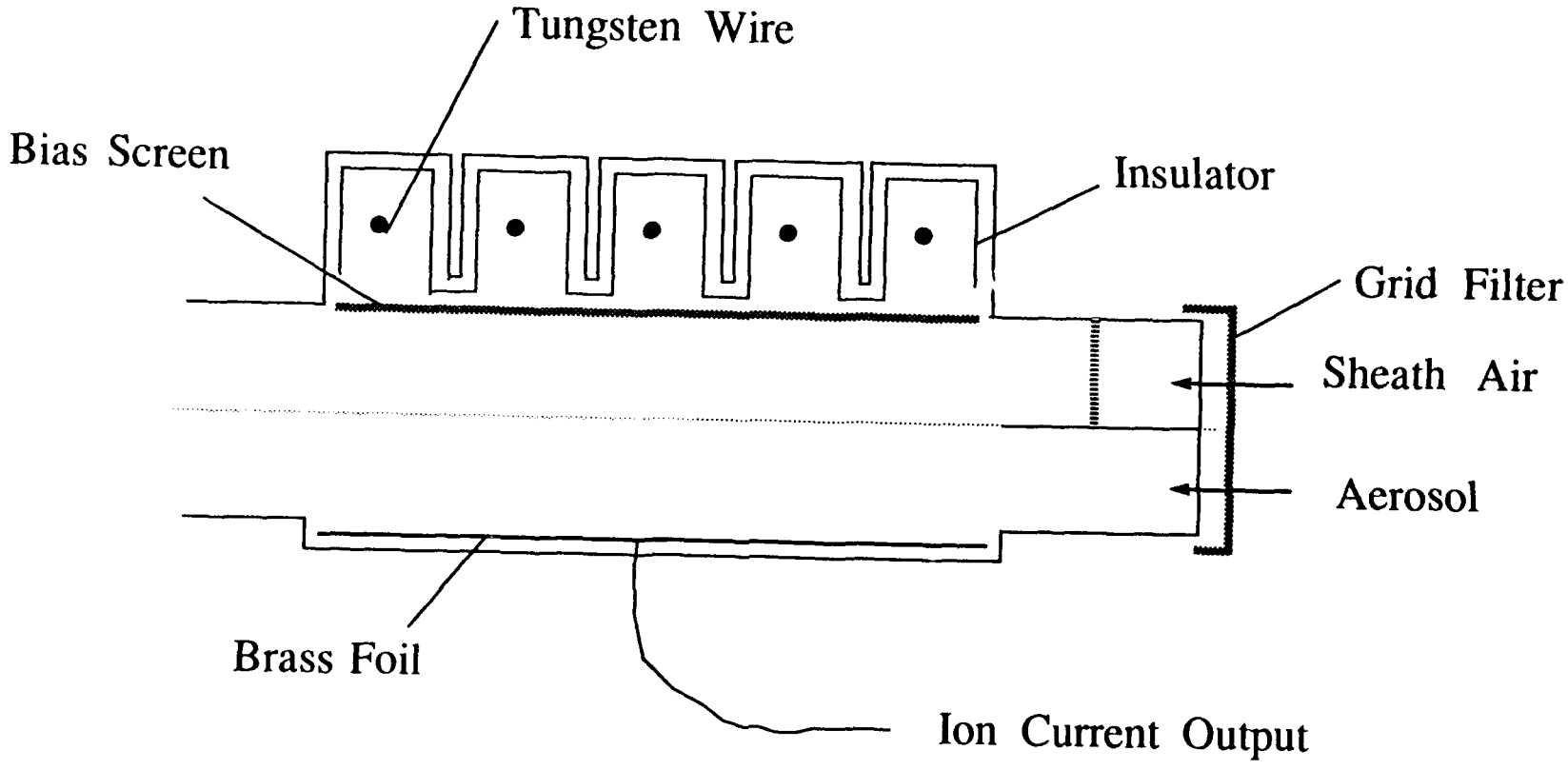

Figure 3.4 Parallel Plate Charger Model with Five Wires

Thus the three key variables in the TSI charger and the prototypes constructed in our laboratory were the voltage on the charging wire , the voltage on the bias screen , and the current measured at the brass foil. These were also the key variables measrued in the parallel plate models shown in figures 3.3 and 3.4. As mentioned above the screen grid size may be a fourth variable.

The parallel plate configurations described in figure 3.3 and 3.4 were designed because particle loss inside the charger was too great when the carbon fibers were used. These fibers have a diameter of $2.0\mu m$ and an average length of over $3000\mu m$. As a result gravitational sedimentation and inertial impaction in the charging section may be significant. In order to minimize fiber loss, the charger was redesigned so that there were no bends or constrictions. The new configuration was essentially flow between two parallel plates, with parallel charged wires inset along the top plate. A sheath air stream as shown in figure 3.4 and 3.5 prevented the long fibers from touching the bias screen and causing charger failure because of shorting. The entrance to the charger was $3.5cm \times 11cm$. The length of the charging wire was 11cm and its diameter was $0.00127cm$ (or $0.0005in$). In typical operation the voltage was $6kV$. The copper bias screen consisted of a grid $0.12cm \times 0.12cm$. The wire thickness of the bias screen was measured and found to be approximately $0.04cm$.

It was found that the charge density of ions in the charger was too low. In order to increase the charging density , the charger was redesigned to include multiple (up to five parallel) wires. This had the effect of increasing the net ion flux by a factor of $3.5 - 4$ without altering the voltage on either the charging

wire or the bias screen.

3.2 Electrostatic Separation

Two types of fibers were used in the experiments. The carbon fibers are long, straight and quite uniform approximately $2\mu m$ in diameter. In the experiments, it was observed that carbon fibers had a few negative charges during the generation processes. Only a portion of the fibers were neutralized and there is a light residual of negative charges on the fibers before they enter the charger. It is also true for the iron fibers and carbon flakes. This was verified by turning off the voltage on the tungsten wire and counting the particle number on positive and negative plates.

An algorithm was developed to determine fiber concentration. The fibers were counted along the lines perpendicular to the flow direction at different locations along the precipitator. It was found out that carbon fibers are quite aligned with the flow direction. The mean fiber length on the precipitator is substantially longer than the mean fiber length on the backing filter with the wire voltage on. By increasing the voltage of the precipitator the collection efficiency increases and the length distribution can be seen from the plates.

The iron fibers are much smaller than carbon fibers both in length and in diameter. At the entrance of the charging section, the average diameter is approximately $0.15\mu m$ and the length range up to several hundred micrometers. At the entrance of the charging section, the polarities on the particles are similar to carbon fibers. Since the iron fibers are much smaller in their sizes, the diffusional charging mechanism is the dominant factor in the charging section.

There is a definite length distribution along the flow direction with longer fibers collected close to the entrance and shorter fibers deposited close to the exit of the precipitator. The density of the iron fibers changed dramatically at front and at the back position in the precipitator. A series of electron micrographs were taken of samples from locations marked in figure 3.5 and are shown in figure 3.6 to 3.8. The results prove that the particles can sorted out by their sizes by electrostatic precipitation. By increasing the precipitator voltage, the length distribution along the flow direction does not change obviously, but the density and the collection efficiency increased.

For carbon flakes, the experimental conditions are similar to those for the iron fibers and the results are also similar.

Five aluminum squares ($5cm \times 10cm$) were mounted along each of the two parallel plates of the precipitator. Although initially it was planned to use polycarbonate strips (i.e. Nucleopore filters) , aluminum squares were adopted so that the electrical field in the precipitation section would not be distorted. The carbon fibers and the large iron fibers were countable with an AO microstar series 10 optical microscope. It was necessary to provide a incident light source so as to provide a contrast between the fibers and the aluminum background - $4.7cm$ diameter nucleopore filter($0.4\mu m$ pore diameter) was mounted after the precipitator. Therefore each experiments fibers were counted on a total of eleven collection surfaces (10 aluminum foils on the surface of the precipitator) and a nucleopore filter after the precipitator. The collection efficiency was calculated by counting the particle deposition on the grounded plate, high voltage and the

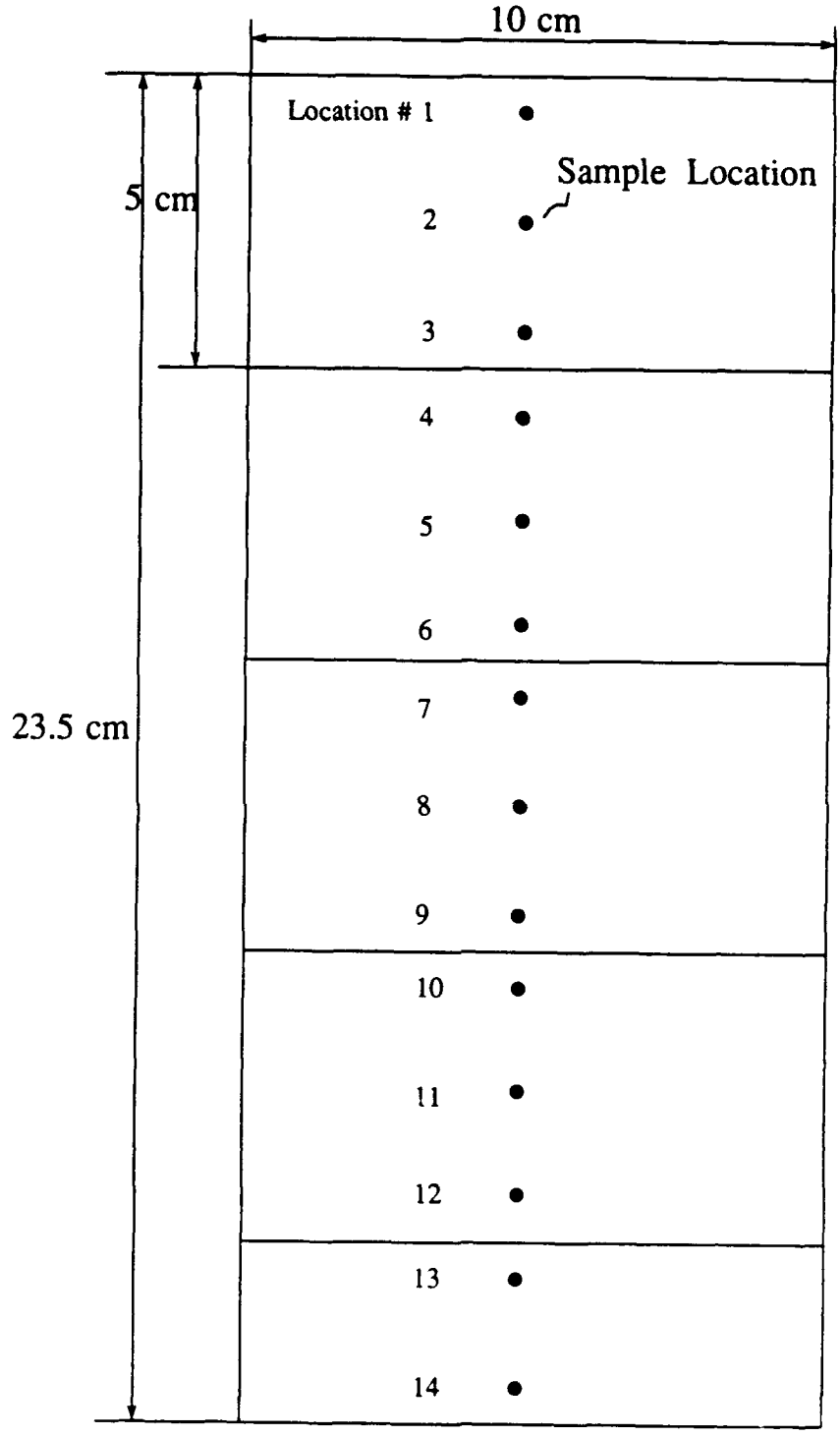

Figure 3.5 Location of Samples for Electron Microscopy

1

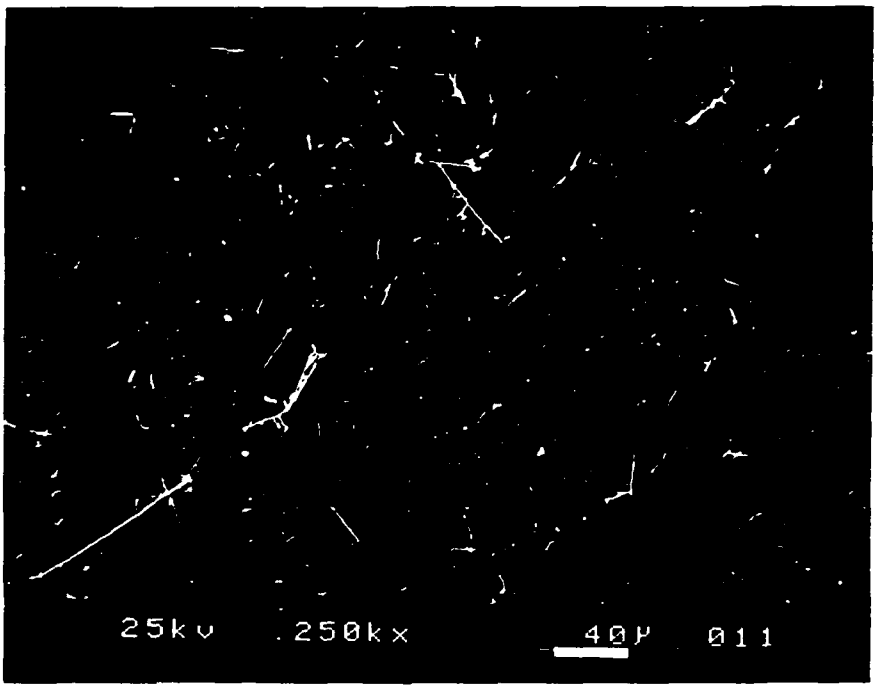

2

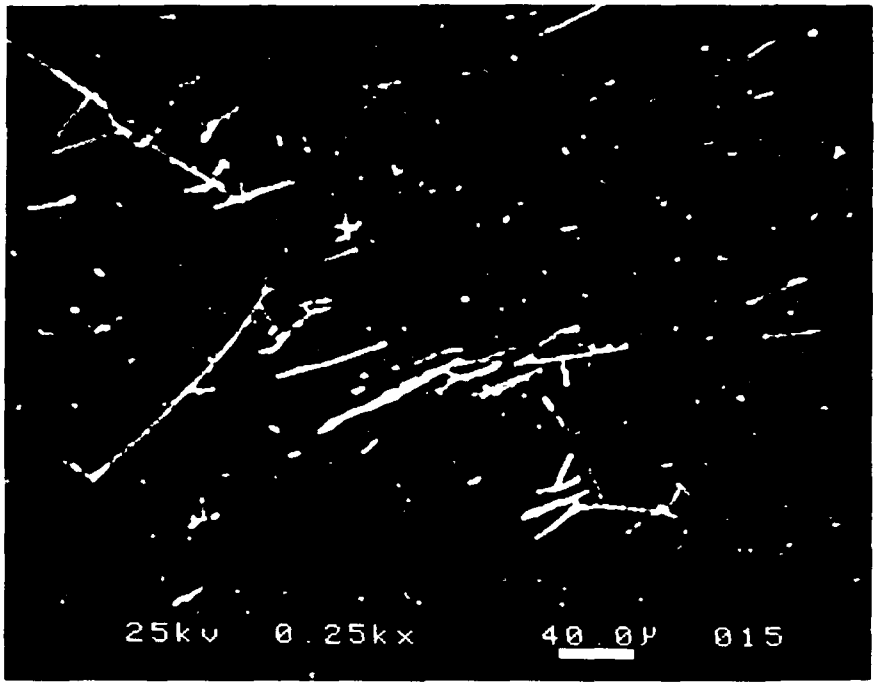

Figure 3.6 Iron Fiber Deposition on Grounded Plate

5

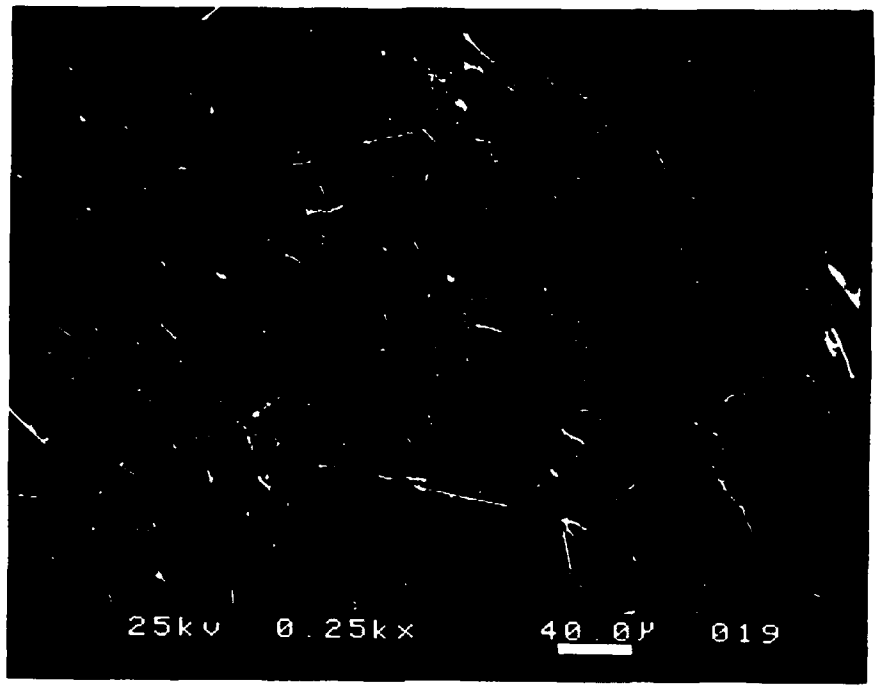

8

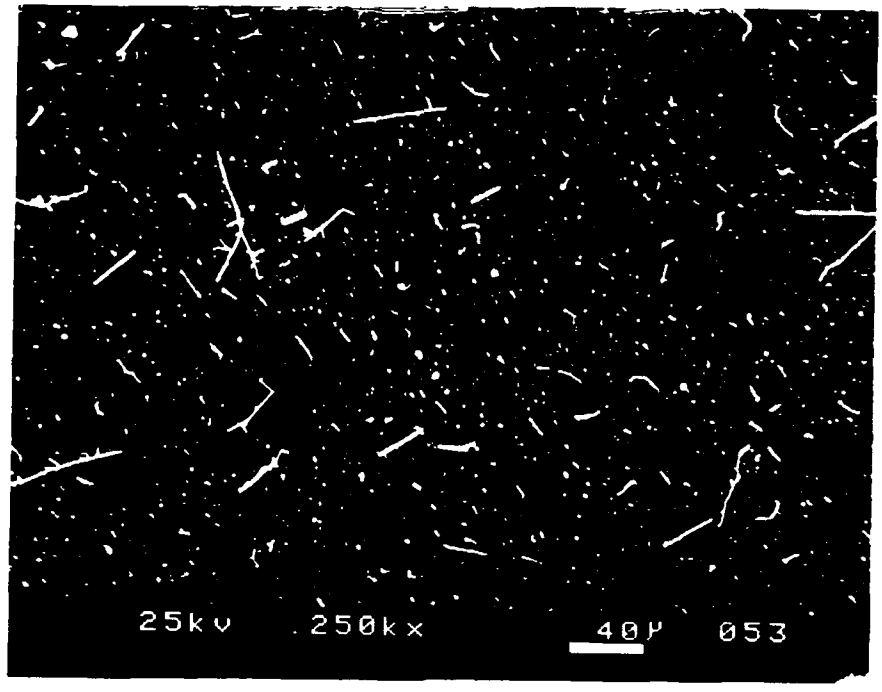

Figure 3.7 Iron Fiber Deposition on Grounded Plate

11

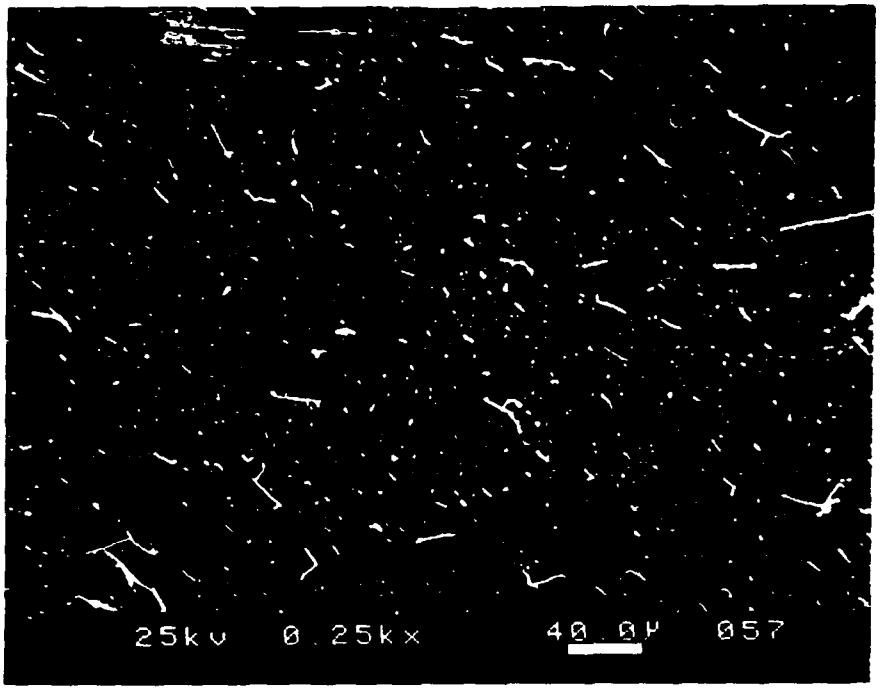

14

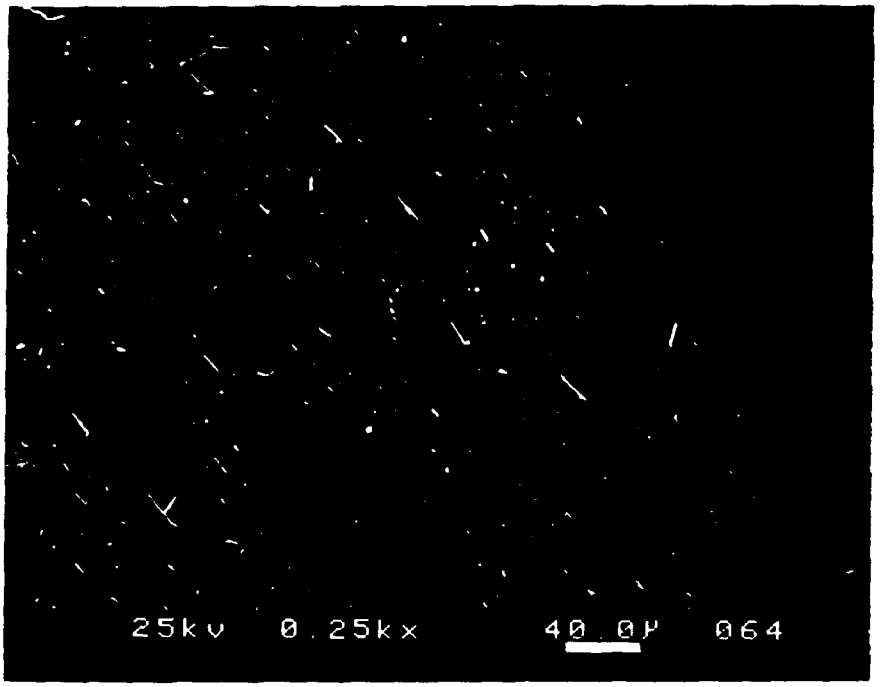

Figure 3.8 Iron Fiber Deposition on Grounded Plate

filter.

$$Efficiency = \frac{N_{Grounded}}{N_{Total}}$$

Experimental Results

In this section we describe a series of experimental investigations. In the preliminary experiments reported here the following variables were considered:

(1) The voltage on the corona wire. In the experiments the values of the voltages ranged from $3kv$ to $7kv$. During each experiment the voltage was maintained constant. In general the experimental measurements were below the point where there was break down and a corona discharge. This implies that there is a potential for a greater charge on the particles.

(2) The voltage on the bias screen. As mentioned above there are two methods by which the efficiency of the unipolar charger might be improved. One is increasing the voltage on the bias screen and the other is decreasing the opening on the bias screen. Only the first approach was investigated in this report. The range of values used was 400 to 800 volts.

(3) The total ion current was increased by increasing the number of corona wires from 1 to 5. This increased the ion current by a factor of $3.5 - 4$ without increasing the voltage on the charging wire or on the grid voltage.

(4) The voltage on the precipitator. In the applications the voltage ranged from 0 to $5kv$.

The conditions and the results of the experiment for carbon and iron fibers are summarized in Table 3.1 and Table 3.2. Results for carbon flakes are sum-

marized in Table 3.3.

The objective of this experiment was to determine if there could be separation according to fiber length and whether there were significant difference in the charge concentration of negative and positive charges. One point is that although charging the fibers did result in more negatively charged particles, there was still a substantial residual of positively charged fibers. Undoubtly the explanations lie in that the fibers are relatively highly charged and that both positive and negative ions are generated in the charger. Our experimental measurements indicate a clear preponderence of ions having one polarity. However at low bias voltages the ion flux is reduced directly by the weaker external electrical field.

3.3 Aerodynamic Separation

Several size classifiers based on aerodynamic separation are commerically available. At least one of them has a documented ability to cut particles below $0.5\mu m$. However the classifier performance is usually limited by the ability to disperse the feed powder in the micrometer and submicrometer size range. An example of the performance of the Nisshin Classifier is indicated in figure 3.9. Starting with a feed glass powder consisting of a $5.21\mu m$ volume median diameter for two size cuts, the fine one with a median diameter of $2.27\mu m$ and the other coarse fraction with a v.m.d. of $11.31\mu m$.

Because of this available information, we did not test the classifier in this Phase I program. However we investigated the effect of aspect ratio in aerodynamic classifier using a mixture of the carbon and iron fibers. The aerodynamic

TABLE 3.1 SUMMARY OF RESULTS FOR CARBON FIBERS

Material	Carbon Fiber			
Voltage on Charging Wire	0.0	0.0	6 kv	6 kv
Voltage on Grid Screen	0.0	0.0	500 v	500 v
Voltage on Precipitator	0.0	3 kv	3 kv	5 kv
Measured Ion Current	0.0	0.0	40 nA	40 nA
Number of Counted Fibers on Positive Electrode	45	80	120	57
Number of Counted Fibers on Negative Electrode	35	34	165	80
Number of Counted Fibers on Backing Filter	100	100	150	136
Mean Fiber Length(*) (Negative Charged)	2083.1	2114.9	1494.4	1280.2
Mean Fiber Length(*) (Positive Charged)	2386.8	1800.7	1251.9	1074.6
Mean Fiber Length(*) (Backing Filter)	627.8	1064.2	624.0	614.1
Collection Efficiency(**)	0.031	0.039	0.569	0.546

* - lognormal distrbution is used.

** - $N_{Grounded} / N_{Total}$

TABLE 3.2 SUMMARY OF RESULTS FOR IRON FIBERS

Material	Iron Fiber			
Voltage on Charging Wire	0.0	0.0	6 kv	6 kv
Voltage on Grid Screen	0.0	0.0	600 v	750 v
Voltage on Precipitator	0.0	3 kv	3 kv	5 kv
Measured Ion Current	0.0	0.0	40 nA	40 nA
Number of Counted Fibers on Positive Electrode	60	635	299	234
Number of Counted Fibers on Negative Electrode	54	277	1114	1655
Number of Counted Fibers on Backing Filter	100	100	100	154
Mean Fiber Length(*) (Negative Charged)	491.4	21.49	28.09	22.75
Mean Fiber Length(*) (Positive Charged)	317.7	28.93	20.12	11.77
Mean Fiber Length(*) (Backing Filter)	33.5	37.14	15.05	17.85
Collection Efficiency(**)	0.00	0.20	0.569	0.939

* - lognormal distribution is used

** - $N_{Grounded} / N_{Total}$

TABLE 3.3 SUMMARY OF RESULTS FOR CARBON FLAKES

Material	Carbon Flake			
Voltage on Charging Wire	0.0	0.0	5.5 kv	6 kv
Voltage on Grid Screen	0.0	0.0	500 v	500 v
Voltage on Precipitator	0.0	3 kv	3 kv	5 kv
Measured Ion Current	0.0	0.0	40 nA	40 nA
Number of Counted Fibers on Positive Electrode		145	69	
Number of Counted Fibers on Negative Electrode		79	218	
Number of Counted Fibers on Backing Filter		12	23	
Mean Fiber Length(*) (Negative Charged)		8.81	9.71	
Mean Fiber Length(*) (Positive Charged)		7.58	12.9	
Mean Fiber Length(*) (Backing Filter)		14.7	10.1	
Collection Efficiency(**)		0.370	0.611	

* - lognormal distribution is used

** - $N_{Grounded} / N_{Total}$

diameter 'D_{ae}' is defined as the diameter of a unit density sphere with the same settling velocity as the particle in consideration. For fibers it is known that

$$D_{ae} = kD_f\beta^{1/6}$$

where k is order of unity. D_f is the end diameter of the fiber and β is the aspect ration - length/diameter of the fiber.

For the carbon fiber with a mean diameter of $3\mu m$, and specific gravity close to 2.0, the aerodynamic diameter for aspect ratios of 1000, 100, and 10 are 13.5, 9, and $6.2\mu m$. For the iron fibers the specific gravity is 7, mean fiber diameter is $0.15\mu m$, and for aspect ratio of 100 the aerodynamic diameter is $0.84\mu m$.

An aerodynamic classifier shown in figure 3.10 based on in-line cyclons (Shaw et al, 1985) designed by University of Minnesota was used to separate the iron fiber and the carbon fiber mixed at a ratio of 1 : 1. Results are summarized in Table 3.4. As expected the carbon fibers were removed in the first three stages and the iron fibers were all collected on the final filter. The observation confirms that fiber diameter, not length, is of main importance and separation based on end diameter is feasible.

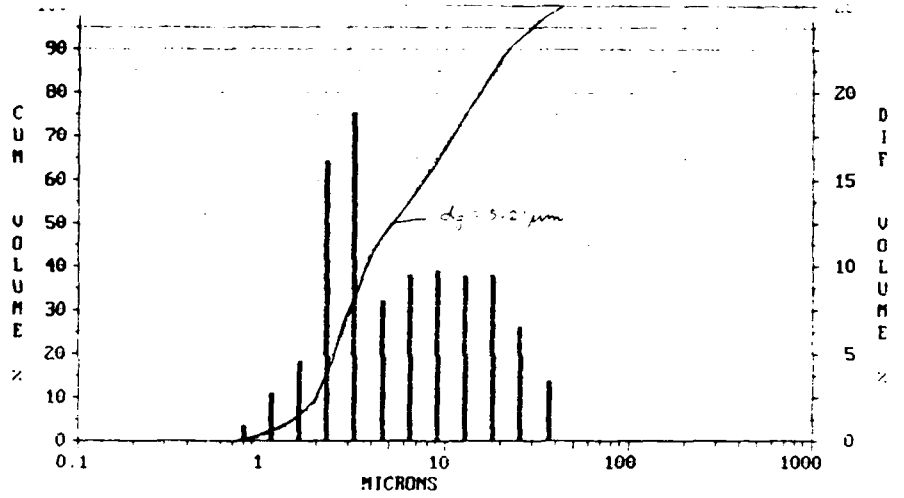

3(a) Feed Powder Size Disribution

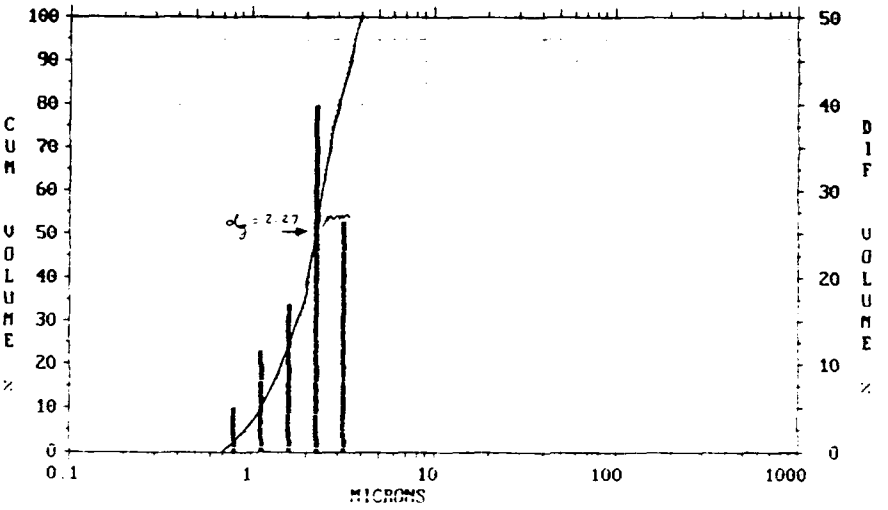

3(b) Fine Size Cut

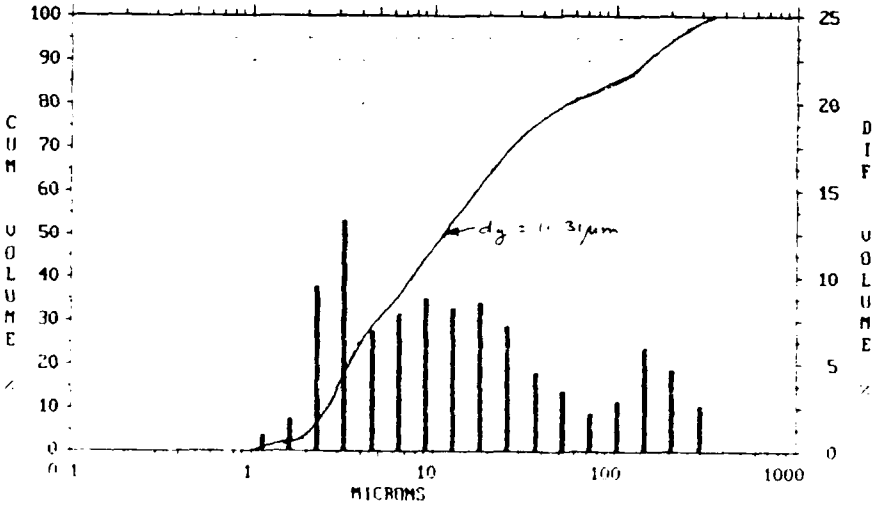

3(c) Coarse Size Cut

Figure 3.9 Nisshin Classifier Performance

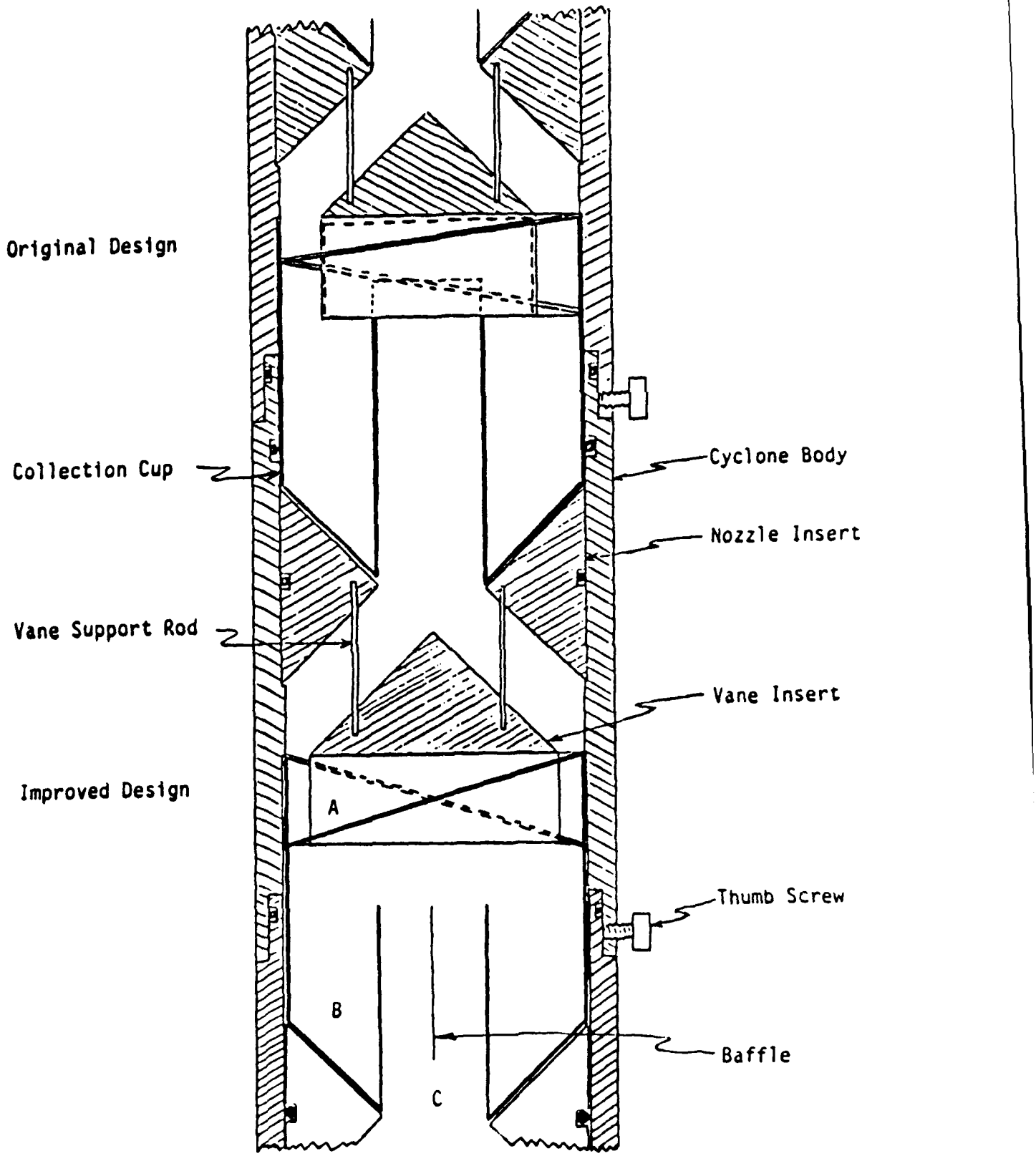

Figure 3.10 Schematic Diagram of the Axial Flow Cyclne(from Shaw et al., 1985)

Table 3.4 Performance of University of Minnesota in-line Cyclones

INPUT 1:1 Mixture of Carbon Fiber and Iron Fiber

30 lpm flow Rate

OUTPUT	Cut Size (μm)	Collection(%) Carbon Fiber	Iron Fiber
STAGE 1	12.2	80	0
STAGE 2	7.9	15	0
STAGE 3	3.6	5	0
STAGE 4	2.05	0	0
STAGE 5	1.05	0	0
FILTER		0	100

4. Conclusions and Recommendations for Phase II Prototype

In this Phase I feasibilty program, theortical development, computer simulation and limited experimental investigation were undertaken to develop a concept for combined tandem aerodynamic and electrostatic sorting of particles. There is strong need to develop a sorting device for high aspect ratio particles such as fibers and flakes. The following points summarize our findings :

1. Theoretical calculations indicate electrostatic sorting of particles by aspect ratio is feasibile.

2. Experimental investigation qualitatively confirms feasiblity.

3. Aerodynamic classifiers are capable of separating 0.5 micrometer sized and large particles.

4. Phase II prototye will employ tandem aerodynamic and electrostatic section.

The Phase II prototype is shown schematically in figure 4.1. A commerical classifier may be used or a special classifier can be designed to cover the size range most important for the intended applications. A corona charger will be used to charge the particles. A battery of alternative positive and negative(grounded) plates will be used to collect high aspect ratio particles. A variable voltage differential will be used to deposit different aspect ratio particles. A rapper arrangement will be used to harvest the desired particles after a powder batch is processed.

Particle Technology, Inc. and the subcontractor University of Maryland

continue to perform additional measurement, necessary before a detailed proposal for Phase II will be submitted.

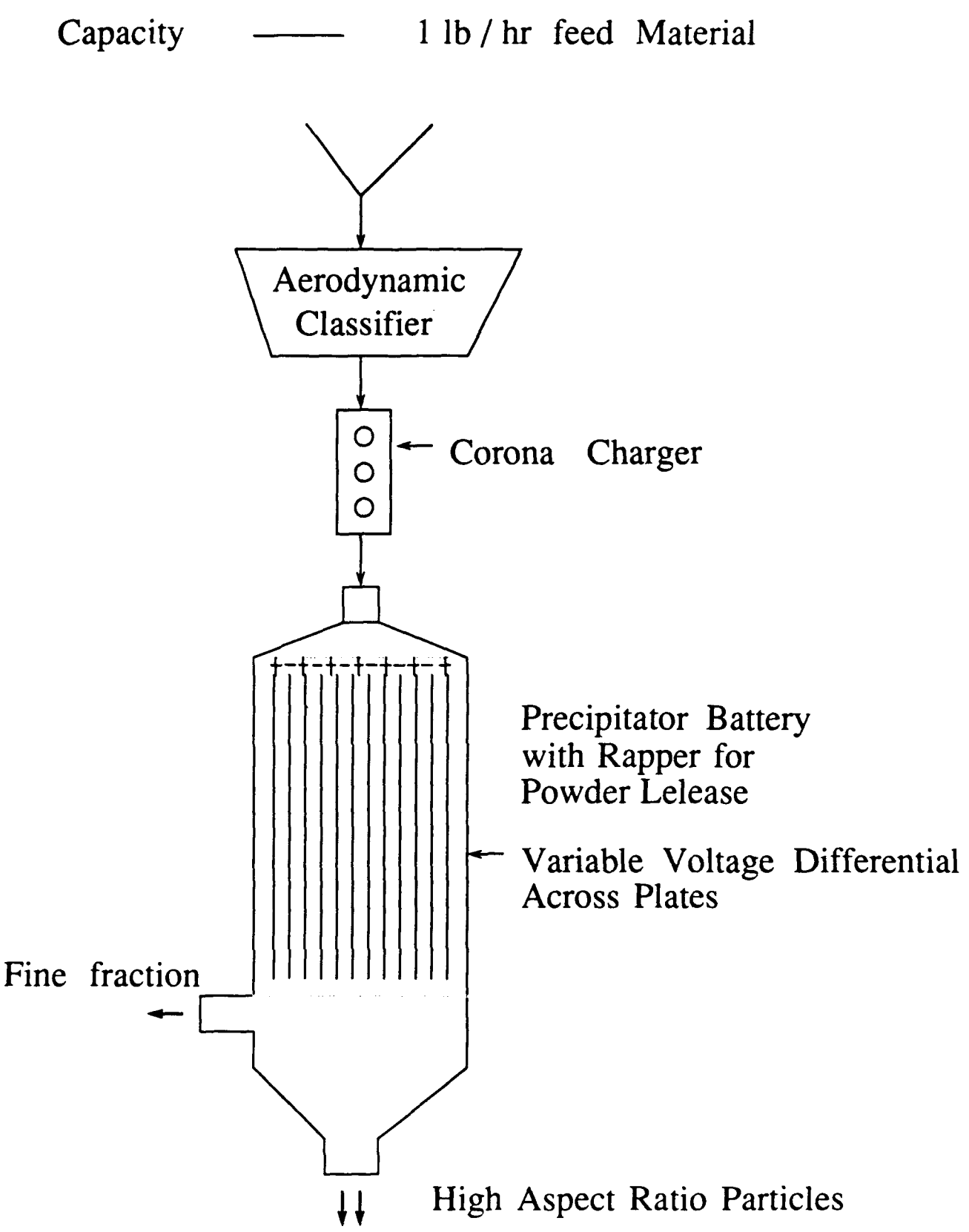

Figure 4.1 Phase II Prototype Schematic

Blank

REFERENCES

Allen, T.(1983) "Particle Size Measurement", Chapman & Hall, London.

Cheng, Y., H. Yeh(1983) J. Aerosol Sci., Vol. 14, pp 489.

Davsion, S.W.(1984) Evaluation of Kinetic Models for the Charging of Ultra-fine Particles by Diffusion of Ions, Ph.D. Dissertation, University of Maryland, College Park.

Fuchs, N.A.(1968) "On the Stationary Chagre Distribution on Aerosol Particles in a Bipolar Ionic Atmosphere", Geofisica Pura e Apllicada, Vol. 56, pp 185-193.

Fuchs, N.A.(1964) The Mechanics of Aerosols, Dover.

Gentry, J.W., J. Brock, J.(1967) J. Chem. Phys., Vol. 47, pp 64.

Gentry, J.W.(1972) "Charging of Aerosl by Unipolar Diffusion on Ions", J. of Aerosol Sci., Vol. 3, pp 65-76.

Gunn, R.(1955) J. of Meteorology, Vol. 11, No. 5, pp 339-347.

Hopple, W.(1978) "Application of Three Body Recombination and Attachment Coefficients to Tropospheric Ions", Pure and Applied Geophysics, Vol. 75, pp 158.

Laframboise, J., J. Chang(1973a) Physics of Fluids, Vol. 16, pp 629.

Laframboise, J., J. Chang(1973b) J. Aerosol Sci., Vol. 8, pp 331.

Leschonski, K.(1987) Powder Technology, Vol. 51, pp 49-59.

Marlowe, W., J. Brock(1975) J. Colloid and Interface Sci., Vol. 51, pp 23.

Shaw, D.T., M.T. Cheng, B.Y.H. Liu, K.C. Rubow(1985) "Inertial Aerosol size

Sample Train", U S Army AMCCOM Report# CRDC-CR-84085.

Yamada, Y. et al(1987) Powder Technology, vol. 50, pp 275.